



HAL
open science

E4F1 deficiency results in oxidative stress-mediated cell death of leukemic cells.

Elodie Hatchi, Genevieve Rodier, Matthieu Lacroix, Julie Caramel, Olivier Kirsh, Chantal Jacquet, Emilie Schrepfer, Sylviane Lagarrigue, Laetitia Karine Linares, Gwendaline Lledo, et al.

► **To cite this version:**

Elodie Hatchi, Genevieve Rodier, Matthieu Lacroix, Julie Caramel, Olivier Kirsh, et al.. E4F1 deficiency results in oxidative stress-mediated cell death of leukemic cells.. *Journal of Experimental Medicine*, 2011, 208 (7), pp.1403-17. 10.1084/jem.20101995 . inserm-00610191

HAL Id: inserm-00610191

<https://inserm.hal.science/inserm-00610191>

Submitted on 21 Jul 2011

HAL is a multi-disciplinary open access archive for the deposit and dissemination of scientific research documents, whether they are published or not. The documents may come from teaching and research institutions in France or abroad, or from public or private research centers.

L'archive ouverte pluridisciplinaire **HAL**, est destinée au dépôt et à la diffusion de documents scientifiques de niveau recherche, publiés ou non, émanant des établissements d'enseignement et de recherche français ou étrangers, des laboratoires publics ou privés.

E4F1 deficiency results in oxidative stress-mediated cell death of leukemic cells

Elodie Hatchi¹, Genevieve Rodier¹, Matthieu Lacroix², Julie Caramel¹, Olivier Kirsh¹, Chantal Jacquet¹, Emilie Schrepfer², Sylviane Laguarrigue², Laetitia Linares², Gwendaline Lledo², Sylvie Tondeur⁴, Pierre Dubus³, Claude Sardet^{1,5} and Laurent Le Cam^{1,2,5}.

¹Institut de Génétique Moléculaire de Montpellier, CNRS UMR5535, Université de Montpellier, IFR122, Montpellier 34293, France

²Institut de Recherche en Cancérologie de Montpellier, INSERM U896, Montpellier, 34298, France.

³Université de Bordeaux, EA2406, Bordeaux, 33076 France.

⁴Laboratoire d'Hématologie, Hôpital St Eloi, CHU, Montpellier, 34295, France.

⁵Corresponding authors: laurent.lecam@inserm.fr (L.L.C.) (contact with the editor) and claude.sardet@igmm.cnrs.fr (C.S.). tel: (33) 4 67 61 23 49; fax: (33) 4 67 61 37 87

Condensed title: E4F1 functions during leukemic development

Key words: E4F1, knock-out, histiocytic sarcoma, leukemic cells, oxidative stress, cell death

Total character count (not including spaces): 40929

Non standard abbreviation list:

3MA, 3 methyl-adenine

4OHT, 4 hydroxy tamoxifen

AML, acute myeloid leukemia

DCFDA, 2',7'-dichlorofluorescein

HS, histiocytic sarcoma

HSC, hematopoietic stem cell

PET, positron emission tomography

ROS, reactive oxygen species

OCR, oxygen consumption rate

shRNA, short hairpin RNA

Abstract (221 words)

The multifunctional E4F1 protein was originally discovered as a target of the E1A viral oncoprotein. Although E4F1 functions remain poorly documented, growing evidences indicate that E4F1 is involved in key signalling pathways that are commonly deregulated during cell transformation. To address the importance of *E4F1* during tumorigenesis, we developed a tumor prone mouse model based on *E4F1* conditional knock-out and *Ink4a/Arf* null alleles. In this model, all mice developed histiocytic sarcomas (HS), a tumor originating from the monocytic/macrophagic lineage. *E4F1* inactivation resulted in cell death of HS cells and tumor regression *in vivo* and expanded the lifespan of those animals. In murine and human HS cell lines, *E4F1* inactivation resulted in mitochondrial defects and increased ROS levels that triggered massive cell death. E4F1 pro-survival functions extend to other myeloid leukemic cells since shRNA-mediated depletion of E4F1 also induced mitochondrial defects and ROS-mediated cell death in several human myeloid leukemic cell lines. Interestingly, these defects were detected in HS cells but not in normal primary macrophages. In addition, E4F1 protein is overexpressed in a large subset of human acute myeloid leukemia (AML) samples, suggesting that leukemic cells rely on *E4F1* as they become transformed. Hence, our data revealed an unexpected role for *E4F1* in cell survival of myeloid leukemic cells and support the notion that targeting E4F1 activities might have therapeutic interest.

Introduction

Pioneer work on viral oncoproteins led to the discovery in the 80^{ies} of several essential regulators of cell division and cell survival. Among those, E4F1 was originally identified as a cellular target of the E1A viral oncoprotein during adenoviral infection, and was originally characterized for its implication in the transcriptional regulation of the viral E4 promoter (Lee and Green, 1987; Lee et al., 1987; Raychaudhuri et al., 1987). In addition to its intrinsic transcriptional activities (Ahmed-Choudhury et al., 2005; Fajas et al., 2001), E4F1 also exhibits an atypical ubiquitin E3 ligase function that targets other transcription factors, including the p53 tumor suppressor (Le Cam et al., 2006). Although the complex transcriptional program regulated by E4F1 remains poorly understood, E4F1 is implicated in several steps controlling cell cycle progression in both somatic and embryonic cells (Fernandes et al., 1998; Le Cam et al., 2004; Rooney, 2001). Furthermore, *E4F1* was recently shown to be essential for epidermal stem cell maintenance and proper skin homeostasis in murine epidermis (Lacroix et al., 2010).

Growing evidences suggest that E4F1 is implicated in carcinogenesis. Consistent with that notion, E4F1 was found to be regulated and/or to interact with several viral oncoproteins, including E1A13S (adenovirus serotype V) (Raychaudhuri et al., 1987), GAM1 (adenovirus Celso) (Colombo et al., 2003), and HBX (Hepatitis virus B) (Rui et al., 2006). In addition, E4F1 is involved in several essential oncogenic pathways, including the RB and p53 tumor suppressor pathways. Indeed, inactivation of *Rb* decreases E4F1 anti-proliferative activities (Fajas et al., 2000), and E4F1 impinges on the p53 pathway at different levels. Thus, through its atypical ubiquitin E3 ligase domain, E4F1 modulates p53 transcriptional activities independently of degradation, and modulates its effector functions involved in alternative cell fates: growth arrest or apoptosis (Le Cam et al., 2006; Sandy et al., 2000). E4F1 also directly

interacts with upstream regulators of the p53 pathway such as the polycomb member Bmi1 (Chagraoui et al., 2006), a transcriptional repressor of the *CDKN2A* locus (also referred to as the *Ink4a/Arf* locus), as well as with one of its encoded proteins, the p14^{ARF} tumor suppressor (Rizos et al., 2003). Finally, E4F1 interacts with the p53 target gene product FHL2/Dra1 that modulates E4F1-p53 binding (Paul et al., 2006).

Although they play important roles in E4F1 associated activities, genetic evidences indicate that *E4F1* functions extend beyond the Rb and p53 pathways. Thus, functional inactivation of either pathway only partly rescues phenotypes associated with E4F1 gain or loss of functions. Consistent with that notion, peri-implantation lethality of *E4F1* KO embryos is not rescued by concomitant inactivation of *p53* (Le Cam and Sicinski, unpublished data), and *E4F1* KO epidermal stem cell defects are partly but not fully rescued upon genetic inactivation of the p53 pathway (Lacroix et al., 2010). Recent data also suggest that E4F1 participates in other oncogenic pathways, as shown by its direct interaction with several tumor suppressors or oncogenes, including RASSF1A (Ahmed-Choudhury et al., 2005; Fenton et al., 2004), HNF1 (Dudziak et al., 2008), SMAD4 (Nojima et al.), and HMGA2 (Tessari et al., 2003). Hence, those interactions raise the question about E4F1 functions that are independent of the Rb and p53 pathways, in particular during tumor development.

Here we started to address the importance of *E4F1* during tumorigenesis, using a mouse model harboring a genetic alteration of the *Ink4a/Arf* locus. By virtue of specific promoters and first exons, this locus generates 2 transcripts with distinct open reading frames encoding the p16^{INK4a} and ARF proteins that exhibit independent but synergistic tumor suppressor activities through their implication in the Rb and p53 pathways, respectively (Kim and Sharpless, 2006; Quelle et al., 1995) (Berger and Bardeesy, 2007) (Kamijo et al., 1997; Sharpless et al., 2001). Loss of the *Ink4a/Arf* locus, or functional inactivation of its encoded

proteins, occurs in a wide spectrum of human tumors, including melanoma, pancreatic adenocarcinoma, glioblastoma, lung cancer, bladder carcinoma, lymphoid and myeloid leukemias (Kim and Sharpless, 2006). In this report, we addressed the direct implication of *E4F1* in leukemic development in a tumor prone mouse model resulting from *Ink4a/Arf* inactivation. In that model, as well as in several human myeloid leukemia cell lines, *E4F1* inactivation resulted in mitochondrial defects and oxidative stress-mediated cell death. In addition, we found that E4F1 is overexpressed in a large subset of human acute myeloid leukemias (AML). Altogether, our data show an important function of *E4F1* in tumor cell survival.

Results

Development of a mouse histiocytic sarcoma model harboring $E4F1$ conditional KO allele.

In order to study $E4F1$ functions during tumorigenesis, we used a recently developed genetically engineered mouse model containing $E4F1$ null and $E4F1$ conditional KO alleles ($E4F1^{\text{flox}}$) based on the Cre/Lox-P technology (Fig. 1 A and Fig. S1A) (Le Cam et al., MCB 2004;(Lacroix et al., 2010)). $E4F1^{\text{flox}}$ mice were crossed with RERT mice, a knock-in (KI) strain expressing the 4-hydroxy-tamoxifen (4OHT)-inducible Cre-ER^{T2} fusion protein under the control of the ubiquitously active promoter of the *RNA polymerase II* large subunit gene (Guerra et al., 2003). *In vivo* recombination efficiency of the $E4F1^{\text{flox}}$ allele was assessed in several organs of $E4F1^{\text{flox}}; RERT^{\text{KI}/\text{KI}}$ mice by quantitative PCR on genomic DNA, RT-qPCR on purified RNA, or western blot analyses of total protein extracts (Fig. 1 B and Fig. S1 A). Upon 4OHT administration, high recombination efficiency was detected in several organs including liver, spleen, lungs, as well as in peripheral white blood cells, and total or purified lineage negative (Lin-) bone marrow cells (Fig. 1 B). These analyses validated our model and confirmed that $E4F1$ is efficiently deleted upon Cre activation in the hematopoietic compartment. However, analyses of $E4F1^{\text{flox}}; RERT^{\text{KI}/\text{KI}}$ mice also revealed critical roles of $E4F1$ in other organs, limiting long-term investigations of phenotypes resulting from $E4F1$ loss in the hematopoietic compartment in that mouse model.

To address $E4F1$ functions during tumorigenesis, we next crossed $E4F1^{\text{flox}}; RERT^{\text{KI}/\text{KI}}$ animals with *Ink4a/Arf* KO mice. The latter strain of mice harbors a deletion of exons 2 and 3 of the *Ink4a/Arf* locus, and therefore expresses neither p16^{INK4a} nor p19^{ARF}. *Ink4a/Arf* null animals are tumor prone, and were previously described to develop with high penetrance essentially B and T cell lymphomas and soft tissue sarcomas with an expected average age of tumor appearance around 30 weeks (Serrano et al., 1996). To avoid defects resulting from $E4F1$ inactivation in the whole organism and investigate $E4F1$ functions

during tumorigenesis, we transplanted fetal liver hematopoietic stem cells (HSC) isolated from $E4F1^{-}/_{\text{floX}}$; $RERT^{KI}/_{KI}$; $Ink4a/Arf^{-}/_{-}$ embryos, or their control $E4F1^{+}/_{\text{floX}}$; $RERT^{KI}/_{KI}$; $Ink4a/Arf^{-}/_{-}$ littermates, into lethally irradiated wild type (WT) recipient mice (herein referred to as $E4F1$ KO or CT; $Ink4a/Arf$ KO mice, according to the genotype of the transplanted cells). We used this strategy to generate several cohorts of tumor prone mice in which $E4F1$ could be acutely inactivated specifically in the hematopoietic system and in tumors derived from those cells upon administration of 4OHT (Fig. S1B).

We then carefully monitored our transplanted mice for perturbations of the hematopoietic system and for tumor susceptibility. Strikingly, we found that our cohorts of transplanted animals, regardless $E4F1$ genotype, and in absence of 4OHT administration, developed with full penetrance histiocytic sarcomas (HS), a tumor type originating from the monocytic/macrophagic lineage, but no B nor T cell lymphomas. These tumors arised as soon as 10 weeks after transplantation, and post-mortem histological analyses indicated that all transplanted animals showed diffuse and/or nodular neoplastic infiltrations in the spleen, liver or lungs. Pathological analyses of tumors recovered from reconstituted animals confirmed that they exhibited all phenotypic and immunologic features reminiscent of human HS, according to the international world health organization (WHO) classification of human tumors (Weiss et al., 2001). HS tumor cells appeared as large cells with abundant eosinophilic cytoplasm and pleiomorphic nuclei with large nucleoli (Fig. 1 C), showed positive immunoreactivity with the histiocytic cell surface markers F4/80 and/or Mac2, and heterogenous staining for the proliferation marker Ki67 (Fig. 1 D and Fig 2B). All tumors stained negative for B and T cell markers (Fig. S1 D), indicating that none of the transplanted animals developed the previously described B or T cell lymphoma spectrum found in $Ink4a/Arf$ KO animals (Serrano et al., 1996). Increased number of F4/80 positive HS cells was also detected by flow cytometry in the peripheral blood between 10 and 20 weeks after transplantation, and indicated the

progression of the disease (Fig. S1 F). Finally, most of these transplanted animals exhibited profound anemia and body weight loss at late stages of tumor progression (data not shown). Death of those animals occurred between 3 and 11 months after transplantation, according to *E4F1* status (Fig. 2 A).

Altogether, these data indicated that we established a novel murine histiocytic sarcoma model based on transplantation of *Ink4a/Arf* null fetal liver HSC. Tumors that developed in that animal model also harbored *E4F1* conditional KO allele, allowing us to address the roles of *E4F1* during tumor development.

E4F1 inactivation results in decreased tumor development and increased life span.

Next, we addressed the consequences of *E4F1* inactivation in transplanted animals. For evaluation of tumor susceptibility, recipient mice were transplanted with fetal HSC cells harvested from genetically matched *E4F1*^{+/flox} or ^{-/flox}; *RERT*^{KI/KI}; *Ink4a/Arf*^{+/+} or ^{-/-} mice (herein referred to as *E4F1* CT or KO; *Ink4a/Arf* WT or KO, according to the genotype of the transplanted cells). In the first experimental group, 4OHT was administered in reconstituted animals 10 weeks after transplantation to allow full reconstitution of the hematopoietic system before Cre-mediated recombination. Administration of 4OHT was then repeated on a monthly basis until the death of the animals (Fig. S1 B).

As depicted in figure 2 A, *E4F1* inactivation significantly increased the lifespan of animals transplanted with *Ink4a/Arf* KO cells, with a median survival time (50% survival) of 28 and 32 weeks in *E4F1* CT and KO animals, respectively. Of note, approximately 20% of *E4F1* KO; *Ink4a/Arf* KO animals exhibited a much longer lifespan, with death occurring up to 12 weeks later than the last *E4F1* CT; *Ink4a/Arf* KO animal. Necropsy and histological studies of all animals, performed at the time of their natural death, indicated that loss of *E4F1*

reduced tumor infiltration in the main sites of HS dissemination including lungs, liver and spleen (Figs. 2 B, S2 B and data not shown). This reduction of tumor infiltration was also illustrated by a 2.5 fold decrease of the median spleen weight (Fig. 2 C) in *E4F1* KO; *Ink4a/Arf* KO when compared to control animals.

These pathological analyses suggested that *E4F1* inactivation delayed tumor development in animals transplanted with *Ink4a/Arf* KO cells. To further confirm *E4F1* impact on tumorigenesis, we set up an independent experimental group for longitudinal studies in which tumor progression was monitored on individual animals by *in vivo* Positron Emission Tomography (PET) imaging. We performed quantitative analyses on 4 independent animals of each genotype (*E4F1* CT or KO; *Ink4a/Arf* KO). Beside classical PET background observed in heart (Fig. S2 A) that precluded analysis of tumor development in lungs, we efficiently followed tumor progression in liver and spleen. As expected, we observed increased PET signal in both liver and spleen of *E4F1* CT, *Ink4a/Arf* KO animals during the time course of the experiment, illustrating the normal progression of the disease. In strike contrast, we found that *E4F1* inactivation, upon 4OHT administration to *E4F1* KO; *Ink4a/Arf* KO animals, resulted in a strong decrease of PET signal, in both liver and spleen (Fig. 3 A-B and Fig. S2C). Consistent with this tumor regression, we observed on tissue sections prepared from *E4F1* KO; *Ink4a/Arf* KO animals that Mac2-positive HS tumor cells exhibited increased TUNEL (terminal deoxynucleotidyl transferase biotin-dUTP nick end labelling) staining, a hallmark of cell death (Fig. 3 C).

Altogether, these analyses revealed that *E4F1* inactivation delayed HS development, increased lifespan in this tumor prone animal model, and induced tumor regression in established HS.

E4F1 inactivation induced massive cell death of HS cells

Our results prompted us to analyze the cellular consequences of *E4F1* inactivation in several HS cell lines that we established from our HS murine model. Flow cytometry and immunofluorescence analyses indicated that the established cell lines expressed predominantly the Mac2 or F4/80 surface markers, with some cell lines expressing both markers, confirming their histiocytic origin (Fig. S4 A and B). Conditional *E4F1* inactivation was induced by addition of 4OHT in the culture medium of *E4F1*⁻/_{flox} HS cell lines (hereafter referred to as *E4F1* CT or KO, according to the absence or presence of 4OHT in the culture medium, respectively), resulting in efficient depletion of the E4F1 protein (Fig. 4 A). *E4F1* inactivation *in vitro* resulted in a dramatic decrease of viable cells 3 days after 4OHT addition. Importantly, *E4F1*⁺/_{flox} HS cell lines remained grossly unaffected by 4OHT treatment, confirming that the decreased number of viable cells observed in *E4F1*⁻/_{flox} cells was not the consequence of 4OHT toxicity but resulted from E4F1 depletion (Fig. 4 A and Fig. S4 C). *E4F1* KO HS cells exhibited no alteration of their proliferation rate or of their mitotic index 4 days after 4OHT addition (Fig. 4 B). However, we observed massive cell death upon *E4F1* inactivation, as shown by increased annexin staining (Fig. 4 C). Consistent with this result, *E4F1* inactivation abrogated the formation of colonies in anchorage independent assays (Fig. 4 D).

Altogether, these data indicated that E4F1 depletion resulted in massive cell death in murine HS cell lines established from primary tumors.

E4F1 inactivation results in autophagic cell death in HS cells

Time lapse video microscopy analyses of *E4F1* KO HS cells showed the apparition of large vacuoles reminiscent of autophagy (data not shown), 3 to 4 days upon 4OHT treatment,

just before cell death occurred. Autophagy is a self-degradation process implicating the lysosomal pathway in which intra-cellular membrane structures engulf altered organelles or aggregated proteins. We sought for additional experimental evidences of autophagy in *E4F1* KO HS cells by several complementary approaches. Transmission electron microscopy indicated the presence of ultrastructural characteristics of autophagic cells, such as double-membraned autophagosomes and autolysosomes, in *E4F1* KO HS cells (Fig. 5 A). Moreover, we observed by immunoblot that *E4F1* inactivation resulted in conversion of cytoplasmic LC3 (LC3-I) protein to the autophagosome membrane bound form of LC3 (LC3-II), a hallmark of autophagy (Fig. 5 B). Finally, increased formation of autophagosomes and autolysosomes in *E4F1* KO HS was visualized by fluorescence microscopy after anti-LC3 or acridine orange stainings, respectively (Fig. 5 C and D).

To determine whether induction of autophagy was the main cause of *E4F1* KO HS cell death, cells were treated with the autophagy inhibitor 3-methyladenine (3MA) that blocks an early step controlling autophagosome formation (Levine and Kroemer, 2008; Mizushima, 2009). 3MA efficiently blocked autophagy and cell death in *E4F1* KO cells, as shown by decreased LC3-II expression and reduced number of annexin positive cells (Fig. 5 B and E). We also evaluated whether apoptosis contributed to cell death occurring upon *E4F1* inactivation. The z-VAD caspase inhibitor had a minor but significant effect on cell death of *E4F1* KO HS cells (Fig. S5 A). Altogether, these results showed that *E4F1* KO HS cells died mainly through autophagic cell death with a minor implication of apoptosis.

Autophagic cell death of E4F1 KO HS cells results from mitochondrial defects and increased ROS levels

Oxidative stress is a well known inducer of autophagy in a variety of cell types including macrophages (Xu et al., 2006). Therefore, we wondered whether autophagy

observed in *E4F1* KO HS cells resulted from increased reactive oxygen species (ROS) levels. *E4F1* KO HS cells exhibited increased staining with the 2',7'-dichlorofluorescein diacetate (DCFDA) probe, a cell permeable fluorescent dye that reacts with a broad spectrum of ROS (Fig. 6 A). Importantly, DCFDA staining in *E4F1* KO HS was not modified by the autophagy inhibitor 3MA, indicating that increased ROS levels resulting from *E4F1* inactivation was not a consequence of autophagic cell death (Fig. S6 A). Consistent with the development of an early and massive oxidative stress in these cells, a robust antioxidant response was detectable early on after *E4F1* inactivation, as illustrated by an increased expression of several antioxidants factors, including the transcription factor NRF2, Catalase, heme-oxygenase 1 (HO1), and the NAD(P)H dehydrogenase quinone 1 (NQO1) (Fig. S6 C-F).

Incubation with probes that detect specific ROS subtypes such as Mitosox and Oxyburst confirmed that the oxidative stress that resulted from *E4F1* inactivation included increased levels of superoxide anions of mitochondrial origin (Fig. 6 A). These data suggested that this organelle could be the main source of ROS detected in *E4F1* KO HS cells. As a read-out of potential mitochondrial alterations in *E4F1* KO HS cells, we next determined their *in situ* oxygen consumption rates (OCR) and ATP levels. Compared to control cells, *E4F1* KO HS cells exhibited a strong increase in O₂ consumption (at all levels, i.e: basal respiration, oligomycin C-sensitive respiration, maximum respiratory capacity) (Fig. 6 B). Strikingly, this strong increase in mitochondrial O₂ consumption was not associated with efficient ATP production since *E4F1* KO HS cells exhibited decreased ATP levels (Fig. 6 C). Since it is well established that various alterations of the electron transport chain functions increase ROS production (Koopman et al.), this strongly suggests that *E4F1* KO HS cells display mitochondrial alterations that impinge on the efficient coupling between oxygen consumption and ATP production, ending in increased ROS production.

The direct consequence of a massive increase in ROS levels is the oxidation of the cellular components, including DNA. Accordingly, we detected increased levels of 8-hydroxy-2'-deoxyguanosine (8-OHdG) in *E4F1* KO HS cells, a stable marker of oxidatively damaged DNA, as shown by nuclear relocalization and increased intensity of the 8-OHdG staining (Struthers et al., 1998) (Fig. 6 D).

These data led us to further investigate whether these ROS were the main cause of death that resulted from *E4F1* inactivation. Treatment of *E4F1* KO HS cells with the superoxide anion scavenger Tiron (4,5-dihydroxy-1,3-benzene disulfonic acid-disodium salt), i) resulted in reduction of the conversion of LC3-I to LC3-II (Fig. 6 E), ii) diminished nuclear labelling of 8-OHdG (Fig. 6 D), iii) and led to a marked decrease in the number of annexin positive cells (Fig. S5 B). Similar results were obtained with 3H-1,2 dithiole-3-thione (D3T), a chemical compound that increases cellular anti-oxidant defenses by increasing NRF2 activities (Zhu et al., 2006) (Fig. 6 E and Figs. S5 B and S6 H). In addition, treatment of *E4F1* KO HS cells in culture with the ROS scavenger N-acetyl-L-cysteine (NAC) rescued cellular viability 3 days after 4OHT addition (Fig. 7 A). Finally, NAC treatment of *E4F1* KO; *Ink4a/Arf* KO animals strongly altered the massive cell death occurring in established HS upon *E4F1* inactivation *in vivo*, as shown by decreased TUNEL staining performed on tissue sections prepared from these animals (Fig. 7 B-C).

Collectively, our data support the notion that *E4F1* inactivation in HS cells results in mitochondrial defects and oxidative stress that lead to autophagic cell death, both *in vitro* and *in vivo*.

Increased ROS levels and cell death do not occur in E4F1 KO primary normal macrophages

Careful monitoring of *E4F1* KO or CT; *Ink4a/Arf* WT animals indicated that *E4F1* depletion did not affect dramatically the different lymphoid and myeloid populations in the

peripheral blood (data not shown) and did not alter the lifespan of those animals over a 12 months observation period in that experimental setting (Fig. 2 A). Therefore, we investigated whether cell death resulting from *E4F1* inactivation in HS cells was specific of transformed cells. To address this question, we inactivated *E4F1* *ex-vivo* in purified intra-peritoneal primary murine macrophages. Although efficient *E4F1* depletion was obtained upon 4OHT addition *ex vivo*, neither increased oxygen consumption, increased ROS levels nor induced cell death were detected in these cells (Fig. 8). These data showed that *E4F1* inactivation resulted in cell death selectively in transformed cells originating from the monocytic/macrophagic lineage but not in normal primary macrophages.

E4F1 depletion results in mitochondrial defects, increased ROS levels and cell death in human myeloid tumor cells

The consequences of *E4F1* depletion in HS cell survival prompted us to evaluate whether the observed defects could be extended to human leukemic cell lines of myeloid origin. We first evaluated the consequences of *E4F1* depletion in U937 cells, a cell line originally isolated from pleural effusion of a patient with HS (Sundstrom and Nilsson, 1976). *E4F1* depletion was achieved by transduction of cells with lentiviruses encoding 2 independent shRNAs directed against human *E4F1*, or a control irrelevant shRNA (Fig. 9 A). *E4F1* depletion in U937 cells resulted in increased ROS levels. Comparable results were obtained in other leukemic cell lines, including the acute promyelocytic leukemia HL60, the acute monocytic leukemia THP1, and the erythroleukemic HEL cell lines (Fig. 9 B and S8 D). Interestingly, similar to murine HS cells, *E4F1* depletion in HEL and HL60 cells resulted in increased oxygen consumption (Fig. 9 C). These defects led to massive cell death, as shown by increased annexin staining (Fig. 9 D).

Altogether, our data suggest that the essential roles of *E4F1* in mitochondrial functions

and cell survival observed in murine HS cells extend to human leukemic cell lines. Based on this conclusion, we next conducted a pilot experiment aiming at evaluating E4F1 expression level in samples isolated from leukemic patients.

E4F1 is overexpressed in a large subset of primary human acute myeloid leukemia samples.

HS is a rare human tumor precluding the analysis of a significant number of samples. Since we found that E4F1 depletion induced comparable defects in several leukemic cell lines of myeloid origin, we evaluated E4F1 expression levels in acute myeloid leukemia (AML), a more common myeloid malignancy. E4F1 protein level was assessed by quantitative immunoblotting on protein extracts prepared from 39 bone marrow biopsies harvested from patients diagnosed with AML. Normal bone marrow samples were used as controls. The vast majority (35/39) of AML expressed E4F1 at higher levels than controls, with a subgroup (9/39) that we defined as strong overexpressors (4 to 13 fold increase above controls) (Fig. 9 E and Fig. S 8C). These data were consistent with our observation that murine HS cell lines exhibit higher amount of E4F1 mRNA and protein levels compared to primary macrophages (Fig. S8 A and B). Hence, this pilot experiment suggested that leukemic cells overexpress E4F1 protein, consistent with the notion that E4F1 is essential for their survival.

Discussion

Although the multifunctional E4F1 protein is involved in essential oncogenic pathways, its exact functions during transformation remain poorly understood. Here, we evaluated *E4F1* functions in tumor development *in vivo*, using an original mouse model based on mice transplanted with genetically engineered HSC harboring *Ink4a/Arf* null and *E4F1* conditional KO alleles. This strategy resulted in the generation of a tumor prone mouse model with unexpected tumor spectrum. Although other murine models based on the *Ink4a/Arf* KO allele have previously been shown to develop mainly lymphomas and sarcomas (Serrano et al., 1996), we failed to detect any pathological evidences of lymphoma development in our transplanted mice. Absence of lymphoma in our experimental model did not reflect differences in genetic backgrounds since genetically matched donor mice developed lymphomas with the expected frequency (Fig. S1E). Strikingly, all our transplanted mice developed HS, a rare neoplasm of the histiocytic lineage with poor prognosis and aggressive clinical course in humans. Most human HS cases previously described were originally misclassified and are now recognized as diffuse large B-cell lymphomas with associated reactive macrophages. However, extensive morphological and immunophenotypical analyses confirmed that the hematopoietic tumors arising in our model are *bona fide* HS, according to criteria published in the WHO classification of human tumors (Weiss et al., 2001). The high penetrance of this tumor type raised the question about the molecular etiology and cell of origin of HS. Consistent with previous reports, our data support the cooperating role of functional alterations of the *Ink4a/Arf* locus and the PI3K pathway in HS pathogenesis in murine models (Carrasco et al., 2006; Eischen et al., 2002; Lund et al., 2002). Indeed, although PTEN protein remained expressed in all HS cell lines established from our murine model, we found clear evidences for a deregulation of the PI3K pathway, as illustrated by a marked increase in the activating phosphorylation of AKT on Ser 473 (Fig. S3). Since only

few relevant HS mouse models exist so far (Carrasco et al., 2006; Eischen et al., 2002; Khoo et al., 2007; Martin-Caballero et al., 2001), the characterization of this new model exhibiting full penetrance and apparent specificity for the development of HS might help to better understand the etiology of this aggressive disease.

Using this tumor prone mouse model, we found that *E4F1* inactivation resulted in massive cell death of transformed cells, tumor regression, and increased life span of the transplanted animals. Nevertheless, *E4F1* KO; *Ink4a/Arf* KO animals still died earlier than *E4F1* KO; *Ink4a/Arf* WT mice. The cause of death of these animals remains unclear. Our data do not support the idea that *E4F1* inactivation induced severe hematopoietic defects compromising the lifespan of those transplanted animals. Detailed necropsy analyses performed with trained pathologists indicated that some, but not all, *E4F1* KO; *Ink4a/Arf* KO animals, exhibited lesions that could reflect massive and rapid cell death of tumor cells in essential organs such as lungs and liver. These defects may have resulted in a severe tissue disorganization and animal death.

To decipher *E4F1* functions in HS cell survival, we next performed extensive analyses in established HS cell lines derived from our animal models. Our previous report indicated that *E4F1* KO embryos display mitotic progression defects followed by cell death at the peri-implantation stage, as illustrated by increased mitotic index and aberrant mitotic figures (Le Cam et al., 2004). Such defects were not observed in HS cells upon acute inactivation of *E4F1*, suggesting that *E4F1* has different functions in various cell types.

Compelling evidences indicate that *E4F1* inactivation in HS cell lines turned on a switch toward autophagic cell death, a process that likely reflects the well documented propensity of cells originating from the macrophage lineage to undergo autophagy in stress conditions (Huang et al., 2009; Xu et al., 2006). Seeking for the stress that had initiated this response, we found that acute *E4F1* inactivation in HS cells led to mitochondrial defects and

increased ROS levels. Importantly, rescue experiments based on ROS scavengers or chemical compounds that increase cellular anti-oxidant defenses indicated that these ROS preceded the autophagic cell death response in *E4F1* KO HS cells. Increased ROS levels observed in these cells likely resulted in deleterious oxidation of many cellular constituents, including proteins, DNA and lipids. Accordingly, we observed that *E4F1* inactivation in HS cells associated with massive genomic DNA oxidation that was largely abrogated upon treatment with ROS scavengers. Furthermore, administration of NAC to *E4F1* KO *Ink4a/Arf* KO animals prevented the massive cell death that was observed *in vivo* upon *E4F1* inactivation in established HS. Preliminary analyses performed by PETscan on a limited number of NAC-treated animals also suggested that ROS scavengers prevented tumor regression induced by *E4F1* inactivation (data not shown).

Those results raised the question about the source of ROS production in *E4F1* KO HS cells. Since E4F1 has been described as an interactor and a regulator of the tumor suppressor p53 (Le Cam et al., 2006), one possibility was that E4F1-depletion had modified some p53 functions leading to increased ROS levels and/or activation of an autophagic response. Indeed, beside its well-documented functions on cell cycle and apoptosis, p53 has been recently shown to directly modulate DRAM, a component of the autophagic machinery (Crichton et al., 2006). Furthermore, transcriptional independent activities of cytoplasmic p53 have also been proposed to regulate autophagy (Tasdemir et al., 2008). Finally, p53 has been described to mediate pro- as well as anti-oxidants effects, likely depending on the intensity of the p53 response. Paradoxically, both have been suggested to participate in its tumor suppressor functions (Vousden and Ryan, 2009). We currently do not favor the hypothesis that activation of p53 is involved in increased ROS levels found in *E4F1* KO HS cells since those cells already harbor an altered p53 pathway resulting from genetic inactivation of the *Ink4a/Arf* locus. In addition, shRNA-mediated depletion of endogenous p53 failed to

modulate increased ROS levels or cell death in *E4F1* KO HS cells (Fig. S7).

Our data rather point to a more direct role of E4F1 in the regulation of mitochondrial activities that impinge on ROS levels. Indeed, increased ROS levels were detected by several ROS sensitive fluorescent probes, including dyes that detect superoxide anions of mitochondrial origin. Our data support the importance of superoxide anions, as a byproduct of mitochondrial defects, in the induction of cell death observed in *E4F1* KO HS cells. Consistent with that notion, we found that *E4F1* inactivation resulted in perturbed mitochondrial oxygen consumption and decreased ATP production, and cell death was partly rescued upon treatment with Tiron that allows detoxification of superoxide anions into less toxic ROS. This is of particular interest in light of our recent data showing that *E4F1* inactivation in murine fibroblasts perturbed expression of several mitochondrial components involved in energetic and metabolic processes (Rodier, Le Cam and Sardet, unpublished data). These data support the notion that high ROS levels in *E4F1* KO cells are the direct consequences of mitochondrial dysfunctions, which in turn induce cell death in HS cells. Furthermore, shRNA-mediated depletion of E4F1 in several human transformed cell lines of myeloid origin resulted in the same sequence of events, suggesting that the role of *E4F1* in those processes is conserved in murine and human leukemic cells.

The role of ROS in tumorigenesis remains controversial. On one hand, many reports describe ROS as inducers of tumorigenesis. On the other hand, previous data have also shown that some cancer cells, including leukemic cells, are more sensitive to increased ROS levels than their non transformed counterparts, opening a window of opportunity for pro-oxidant anti-cancer treatments (Huang et al., 2000; Trachootham et al., 2008; Trachootham et al., 2006; Valko et al., 2007). Our data are consistent with the latter strategy since we found that *E4F1* inactivation induces ROS-mediated cell death in HS transformed cells but not in normal primary macrophages. The molecular mechanisms that are responsible for the higher

sensitivity of cancer cells to increased ROS levels still remain unclear. Several explanations have been proposed, implicating the lower anti-oxidant defenses in some tumor cells or the paradoxical role of AKT in sensitizing cancer cells to ROS-induced cell death (Huang et al., 2000; Nogueira et al., 2008). Based on our data showing that transformed, but not normal cells, display mitochondrial defects upon E4F1 depletion, we also do not exclude the possibility that transformed cells exhibit deregulation of some, yet unidentified, mitochondrial activities, that sensitize cancer cells to E4F1 depletion. Together with our finding that overexpression of E4F1 protein level, ranging from moderate (2 to 4 fold) to high (4 to 13 fold), occurs in a large subset of AML samples, these observations raise an interesting hypothesis that some leukemic cells become addicted to the pro-survival functions of E4F1 during the process of cell transformation. In conclusion, our findings may have important implications for novel anti-cancer therapies, in particular for treatment of leukemias that have been shown to respond to chemotherapeutic agents that regulate the redox status.

Materials and Methods

Generation of mutant mice and *E4F1* inactivation *in vivo*.

E4F1 null (Le Cam et al., 2004), *E4F1 flox* (Fig. S1), *RERT* (Guerra et al., 2003), and *Ink4a/Arf* (Serrano et al., 1996) mutant mice were intercrossed to obtain appropriate genotypes: *E4F1*^{+/flox} or ⁻/_{flox}; *RERT*^{KI/KI}; *Ink4a/Arf*^{+/+} or ⁻/₋. The mice were maintained on a mixed 129Sv/J/DBA/C57BL/6 background. *In vivo* recombination of the *E4F1 flox* allele was obtained by topical skin applications of 4OHT (Sigma) on shaved back skin of the transplanted recipient animals (2mg/mouse/application, 3 applications). For survival analyses, 4OHT administration started 10 weeks after transplantation and was repeated on a monthly basis throughout the entire life of the animals. For PETscan analyses, 4OHT (2mg/mouse/application, 3 applications) was administrated around 20 weeks post transplantation, when animals exhibited obvious signs of tumor development. For NAC based *in vivo* experiments, NAC was administrated at the final concentration of 40 mM in the drinking water (changed every day) for 7 days prior to 4OHT administration, and maintained afterward during the total duration of the experiment (15 days). All animal husbandry and experiments were approved by and performed in accordance with the guidelines of a regional ethic committee.

Transplantation experiments

Congenic C57BL/6-Ly5.1 mice were lethally irradiated (11 Gy) with a cobalt radiation source, and used as recipient mice. 5 x 10⁶ fetal livers donor HSC isolated from Ly5.2 *E4F1* - ⁻/_{flox} or ⁺/_{flox}; *RERT*^{KI/KI}; *Ink4a/Arf*^{+/+} or ⁻/₋ E14.5 embryos, were injected intravenously into the

tail vein of recipient (Ly5.1) mice. Peripheral blood was obtained from retro-orbital sinuses of recipient mice under isoflurane anesthesia and analyzed every 4 weeks after transplantation by flow cytometry with several combinations of lineage specific antibodies: APC-CD19 for B cells, PerCP-CD3 for T cells, APC-Gr1, FITC-F4/80 or PE-Mac2 for myeloid cells. PE-CD45.1 (Ly5.1) and FITC-CD45.2 (Ly5.2) antibodies were used to determine the level of reconstitution by identifying the proportion of donor cells in recipient mice. Fluorochrome-conjugated antibodies used for flow cytometry analyses (FACSCalibur flow cytometer, BD Biosciences) were purchased from BD Biosciences and eBioscience. Flow cytometry data were analyzed with FlowJo software (TreeStar, Inc).

Quantitative RT-qPCR

E4F1 mRNA expression was evaluated in different hematopoietic compartments by RT-PCR. Cells were lysed in TriZol Reagent (Invitrogen) and total RNAs were isolated according to the manufacturer's recommendations. cDNAs were synthesized from 1 μ g of total RNA using random hexamers and SuperScript™ III Reverse Transcriptase (Invitrogen). Quantitative real-time PCR was performed on a LightCycler 480 SW 1.5 apparatus (Roche) with Platinum Taq DNA polymerase (Invitrogen) and a SYBR Green mix containing 3 mM MgCl₂ and dNTPs 30 μ M each; 45 cycles of 95°C for 4 s, 62°C for 10 s, and 72°C for 30 s. Results were quantified with a standard curve generated with serial dilutions of a reference cDNA preparation. PCR products were always loaded on an agarose gel to verify fragment size and purity of amplicons. *RPL13A* and *HPRT* transcripts were used for normalization. Primers sequences were as follows: *E4F1* forward, 5'-CCAAAGCCTACCTGCTCAAG-3' and reverse, 5'-CTGGGCATTCTTGGTTTTGT-3'; *RPL13A* forward, 5'-GAGGTCTGGGTGGAAGTACCA-3' and reverse, 5'-TGCATCTTGGCCTTTTCCTT-3';

HPRT forward, 5'-AAGCCTAAGATGAGCGCAAG-3' and reverse, 5'-TTACTAGGCAGATGGCCACA-3'.

Histology and immunohistochemistry

Formalin-fixed tissues were embedded in paraffin, sectioned and processed for routine H&E staining and immunohistochemistry (IHC). Anti-Ki67 (SP6) and -MPO (Ab-1) antibodies were obtained from Labvision. Anti-CD3- ϵ (M-20) and -Pax5 (C-20) antibodies were obtained from Santa Cruz and anti -F4/80 (BM8) and -Mac2 (M3/38) antibodies from eBioscience. IHC was performed on 4 μ m tissue sections using appropriate primary antibodies and the corresponding biotinylated secondary antibody coupled to streptavidin-peroxidase complex (ABC Vectastain kit, Vector Laboratories). Revelation was performed using the peroxidase substrates DAB (brown coloration) or VIP (dark purple coloration) from Vector Laboratories. TUNEL staining was performed according to the manufacturer (Roche) instructions.

PET-scan analyses

PET-scan analyses were performed at the Animage imaging department in Lyon (CERMEP, France). Animals analyzed by PET imaging belong to an experimental group composed of transplanted animals (4 months post-transplantation) that displayed palpable tumors in spleen, and high percentage of F4/80 positive HS cells in the peripheral blood. Quantitative PET analyses of 4 independent animals of each genotype were performed on spleen and liver before (D0) and after (D15) *E4F1* inactivation. Clinical grade radiolabelled fluoro-deoxy-glucose (^{18}F -FDG) was produced locally using a cyclotron. ^{18}F -FDG-uptake was calculated

from a whole body acquisition of 30 min length on anesthetized animals performed with a high-resolution small animal PET scanner (Raytest ClearPET developed by Crystal Clear Collaboration) after i.v. injection of 300 μCi ^{18}F -FDG in 100 μl 0.9% NaCl solution in tail vein. Acquisition started 2 h after ^{18}F -FDG -injection to reduce tracer uptake in the bladder caused by renal excretion. PET-scan images were reconstructed and quantified according to the injected amounts of ^{18}F -FDG using the freeware Amide.

Reagents

Acridine orange (AO), 3-methyladenine (3MA), 4-hydroxy-Tamoxifen (4OHT), DAPI (4,6-diamidino-2-phenylindole), propidium iodide (PI), Tiron (4,5-dihydroxy-1,3-benzene disulfonic acid-disodium salt), collagenase, HEPES, sodium pyruvate, Tween-20 and NAC were purchased from Sigma. 3H-1,2 dithiole-3-thione (D3T) was purchased from Axxora Platform; Click-it EdU flow cytometry assay kit from Invitrogen, and CM-H₂DCFDA, MitoSOX, Oxyburst and FITC-conjugated avidin were purchased from Molecular Probes. Annexin-V-FLUOS (herein referred to as annexin) and bovine serum albumin (BSA) were purchased from Roche. RPMI Glutamax-I and Fetal Bovine Serum (FBS) were purchased from Gibco and Biowest, respectively.

For experiments on HS cell lines and primary macrophages, the working concentrations of the following chemical reagents were used: AO, 1 $\mu\text{g}/\text{ml}$; 3MA, 1mM; 4OHT, 3 μM , Tiron, 100 μM ; NAC, 200 μM and D3T, 10 μM .

Viability, proliferation, cell death and ROS detection assays

Viability was determined by manual counting after trypan blue exclusion. The proliferation rate of HS cells was assessed after incubation for 2 hours with EdU by FACS analysis with the EdU flow cytometry assay kit, according to the manufacturer recommendations. Mitotic cells were identified with the Ser10 phospho-histone H3 antibody (Cell Signaling Technology). Cell death was evaluated by flow cytometry upon annexin/PI staining. Total and mitochondrial ROS levels were evaluated by flow cytometry or immunofluorescence microscopy, upon staining with CM-H₂DFCDA, Oxyburst and MitoSOX probes, respectively, according to the manufacturer recommendations. As shown in Fig. 6 A (right panel), the kinetics of MitoSOX staining were evaluated over a 75min period. Quantitative data represent the fold increase of time dependent changes in mean fluorescence intensity of MitoSOX staining measured by flow cytometry. Annexin/PI and CM-H₂DFCDA/MitoSOX analyses were performed on freshly trypsinized live cells on a FACSCalibur flow cytometer (BD Biosciences).

Isolation of HS cell lines and primary macrophages

4 HS cell lines (2 *E4F1*^{+/*fl*ox} and 2 *E4F1*^{-/*fl*ox}) were established *ex-vivo* out of 9 lungs and 0 out of 9 livers harvested from unrecombined *E4F1* KO or CT; *Ink4a/Arf* KO animals, as follows: fresh HS of appropriate genotype were harvested from transplanted recipient mice of approximately 20 weeks of age, mechanically dissociated, digested in collagenase for 2 hours at 37°C, and then cultured in RPMI Glutamax-I supplemented with 10% IFBS, 2.5g/L Glucose, 10mM HEPES and 1mM sodium pyruvate in a humidified 5% CO₂, 37°C incubator. Primary macrophages were harvested by injection of 10 ml of PBS in the intraperitoneal cavity of mice of appropriate genotype, centrifuged and plated for 2 hours. Non adherent cells were removed by repeated washing with culture medium. Purity (above 90%) of the adherent

macrophage population was evaluated by flow cytometry with Mac2 antibody. Primary macrophages were cultured in the same conditions and medium than HS cells lines. *E4F1* inactivation in HS cell lines and primary macrophages was obtained by addition of 4OHT to the culture medium, 2 hours after plating.

Measurement of oxygen consumption and ATP production

Oxygen consumption was determined by 2 independent methods. The Seahorse XF24 Extracellular Flux Analyzer (Seahorse Bioscience, North Billerica, MA), based on fluorimetric sensors, was used for real time *in situ* measurement of oxygen consumption rate (OCR) in *E4F1* HS cells and primary intra-peritoneal macrophages. Analyses were conducted on 80,000 cells / well in triplicate for each cell type (*E4F1* CT or KO HS cells or primary macrophages). Mean values of OCR were then calculated following correction to total amount of cellular protein per well. For these experiments, cells were incubated for 1h at 37°C in HCO₃-free DMEM containing 25 mM glucose and 1 mM pyruvate. Measurement of OCR was performed over 2 min in three measurement intervals to assess basal metabolic rate, oligomycin C (1µg/ml final)-sensitive OCR associated to ATP production, and maximal respiratory capacity (upon FCCP (0.3 µM final) followed by rotenone (0.1 µM final) administration). Oxygen consumption was also measured using a temperature-regulated Clark-type O₂ electrode chamber (Strathkelvin Instruments, Glasgow, UK) in murine *E4F1* HS cells and human leukemic cell lines. Oxygen consumption was measured on 5 millions of cells for 5-15 min (until oxygen consumption ceased) at 37°C in presence of 2,5 mM malate and 10 mM pyruvate, upon repeated ADP injection (3 injections of ADP, 1mM final). Respiration values were normalized to cell number. For ATP measurements, 20,000 cells were plated in quadruplicates in a 96 well plate and ATP was measured 3 hours later by using

the Cell Titer Glo (Promega) luminescent assay. Briefly, cells were incubated in the lysis buffer and the luminescence determined 10 minutes later. ATP levels were normalized to total protein levels.

Soft agar assays

Single cell suspensions of HS cells were mixed with RPMI containing 0.4% noble agar and plated on the top of a layer containing 1% noble agar in 6-well plates in triplicate (100,000 cells per plate). Fresh medium, with or without 4OHT, was added every three day. Colonies were stained after 3 weeks of culture with a 0.5% crystal violet solution and counted.

Immunofluorescence microscopy

In all experiments, HS cells were grown on a glass culture chamber (BD-Falcon). For LC3 immunostaining, cells were fixed with 2% paraformaldehyde (PFA) for 5-10 min at room temperature (RT), permeabilized by 0.1% Triton X-100 for 5 min at RT, incubated for 1 hour with a blocking solution of PBS-1.5% BSA, and then stained for 1 hour at 37°C with anti-LC3 antibody (Sigma) or overnight at 4°C with anti-catalase (Rockland), -HO1 (Stressgen), NQO1 (Abcam), anti-NRF2 (generous gift from Schmidt EE, Montana, USA) antibodies. After three washes in PBS- 1% BSA-0.1% Tween-20, the slides were incubated for 45min at 37°C in the dark with FITC-conjugated anti-rabbit secondary antibody. To visualize oxidized DNA (8-hydroxy-2'-deoxyguanosine (8OH-dG) staining), cells were fixed with methanol at -20°C for 20 min and then incubated with FITC-conjugated avidin (15µg/ml) for 1 hour at 37°C, as previously described (Radisky et al., 2005). To detect Mitochondrial ROS, living

cells were first incubated with MitoSOX (5 μ M final) for 10 min at 37°C, and then fixed with 2% PFA. Acidic vesicular organelles (AVOs) were visualized by staining cells with AO (1 μ g/ml) for 10min at 37°C. All fixed cells were co-stained with DAPI for 5 min and mounted in Vectashield imaging medium (Vector Laboratories) before observation with an upright Zeiss Axioimager Z1 / apotome microscope. MitoSOX images were acquired with a gamma adjustment of 0.55.

Quantitative Immunoblotting

Total protein extracts were prepared by lysing HS cells or intraperitoneal primary macrophages in Triton X-100 lysis buffer (50 mM Tris-HCl, pH 7.4, 100 mM NaCl, 50 mM NaF, 5 mM EDTA, 40 mM β -glycerophosphate, 1 mM sodium orthovanadate, 10⁻⁴ M PMSF, 10⁻⁶ M leupeptin, 10⁻⁶ M pepstatin A, 1% Triton X-100), and separated by SDS–polyacrylamide-gel electrophoresis and transferred to nitrocellulose membranes. Membranes were blocked in TBS containing 5% nonfat milk for 1 hour at RT, and incubated overnight at 4°C with primary antibodies. The E4F1 affinity purified rabbit polyclonal antibody was generated against the human full length (aa 1-784) E4F1 protein fused to GST. Anti-actin and anti-LC3 antibodies were purchased from Sigma, anti-GAPDH from Santa-Cruz, DyLight™ conjugated secondary antibodies from Pierce. Quantitative immunoblots were performed using the Odyssey infrared imaging system (LiCor).

Transmission Electron Microscopy and Ultrastructural evaluation

Adherent HS cells were fixed in 3.5% glutaraldehyde in Sorensen's phosphate buffer (0.1M, pH 7.4) for 1 hour at RT. The cells were then scrapped and maintained overnight at 4°C in this fixative solution. After washes in Sorensen's buffer, cells were post-fixed in a 1% osmic acid plus 0.8% potassium ferrocyanide for 2 hours at room temperature in the dark. After two washes in Sorensen's buffer, the cells were dehydrated in a graded series of ethanol solutions (30-100%) and embedded in EmBed 812 resin. Thin sections (85 nm) were cut on a Leica-Reichert Ultracut E ultramicrotome and collected at different levels of each block. These sections were counterstained with uranyl acetate and examined on Hitachi 7100 transmission electron microscope.

Lentiviral particles productions and infections

Viral particles were produced in HEK 293T cells by standard procedures after transfection of the following constructs: pLKO1 encoding shRNAs directed against human E4F1 (shE4F1#1, Sigma mission clone 1740s1c1; shE4F1#2, clone 2411s1c1), or an irrelevant shRNA (shCt, clone shc002). 48 hrs after transfection, viral particles were harvested in the supernatant and added in the culture medium of U937, HEL, HL60, THP1 cell lines in presence of polybrene (8µg/ml final). ROS levels and cell death were evaluated 5 to 7 days after the infection by flow cytometry upon incubation with CM-H₂DCFDA or annexin/PI.

Human samples for E4F1 expression levels evaluation

Anonymous normal and AML bone marrow samples were provided by the CHU St Eloi (Montpellier, France) hematology laboratory (collection number DC-2008-417). Frozen vials

were thawed in complete medium and whole-cell extracts were prepared in Laemmli buffer containing protease inhibitors. E4F1 and actin protein expression levels were determined by quantitative immunoblotting.

Statistic analyses

Unless otherwise indicated, the unpaired Student's *t* test was used in all analyses, data in bar graphs are represented as mean \pm SEM, and statistical significance was expressed as follows:

*, $P < 0.05$; **, $P < 0.01$; ***, $P < 0.001$; ns, not significant.

Acknowledgments:

We thank the RHEM histology facility and Patricia Cavelier for processing our animal tissues; ANIMAGE *in vivo* imaging core facility (Lyon, France) for PET scan analyses, Montpellier Rio Imaging for cell imaging and the CRIC facilities for ultrastructure microscopy (Montpellier, France). We thank Eric Jouffre, Marc Plays and Karim Chebli for technical help in mouse handling; M. Barbacid and M. Serrano for providing us with the *Ink4a/Arf* KO and *RERT* KI strains of mice; S. Pattingre and Lucille Espert for valuable discussions on autophagy; S. Thevenin for statistical analyses. We are grateful to all members of the LLC, CS and L. Fajas laboratories for helpful discussions and critical readings of the manuscript. This work was supported by the Agence Nationale pour la Recherche (ANR), the Association pour la lutte contre le Cancer (ARC), the Leukemia Program from the Fondation de France, the British AICR foundation, by la Fondation pour la Recherche Médicale (CS équipe labélisée 2007) and the institutional supports of the INSERM Avenir Program (LLC) and the CNRS (CS). EH and JC are supported by an ARC PhD and AICR post-doctoral fellowships, respectively. The authors have no conflicting financial interests.

References

- Ahmed-Choudhury, J., A. Agathangelou, S.L. Fenton, C. Ricketts, G.J. Clark, E.R. Maher, and F. Latif. 2005. Transcriptional regulation of cyclin A2 by RASSF1A through the enhanced binding of p120E4F to the cyclin A2 promoter. *Cancer Res* 65:2690-2697.
- Berger, J.H., and N. Bardeesy. 2007. Modeling INK4/ARF tumor suppression in the mouse. *Curr Mol Med* 7:63-75.
- Carrasco, D.R., T. Fenton, K. Sukhdeo, M. Protopopova, M. Enos, M.J. You, D. Di Vizio, C. Nogueira, J. Stommel, G.S. Pinkus, C. Fletcher, J.L. Hornick, W.K. Cavenee, F.B. Furnari, and R.A. Depinho. 2006. The PTEN and INK4A/ARF tumor suppressors maintain myelolymphoid homeostasis and cooperate to constrain histiocytic sarcoma development in humans. *Cancer Cell* 9:379-390.S1535-6108(06)00115-2 [pii] 10.1016/j.ccr.2006.03.028.
- Chagraoui, J., S.L. Niessen, J. Lessard, S. Girard, P. Coulombe, M. Sauvageau, S. Meloche, and G. Sauvageau. 2006. E4F1: a novel candidate factor for mediating BMI1 function in primitive hematopoietic cells. *Genes Dev.* 20:2110-2120.
- Colombo, R., G.F. Draetta, and S. Chiocca. 2003. Modulation of p120E4F transcriptional activity by the Gam1 adenoviral early protein. *Oncogene* 22:2541-2547.
- Crichton, D., S. Wilkinson, J. O'Prey, N. Syed, P. Smith, P.R. Harrison, M. Gasco, O. Garrone, T. Crook, and K.M. Ryan. 2006. DRAM, a p53-induced modulator of autophagy, is critical for apoptosis. *Cell* 126:121-134.S0092-8674(06)00759-8 [pii] 10.1016/j.cell.2006.05.034.

- Dudziak, K., N. Mottalebi, S. Senkel, E.L. Edghill, S. Rosengarten, M. Roose, C. Bingham, S. Ellard, and G.U. Ryffel. 2008. Transcription factor HNF1beta and novel partners affect nephrogenesis. *Kidney Int* 74:210-217.ki2008149 [pii] 10.1038/ki.2008.149.
- Eischen, C.M., J.E. Rehg, S.J. Korsmeyer, and J.L. Cleveland. 2002. Loss of Bax alters tumor spectrum and tumor numbers in ARF-deficient mice. *Cancer Res* 62:2184-2191.
- Fajas, L., C. Paul, A. Vie, S. Estrach, R. Medema, J.M. Blanchard, C. Sardet, and M.L. Vignais. 2001. Cyclin A is a mediator of p120E4F-dependent cell cycle arrest in G1. *Mol Cell Biol* 21:2956-2966.
- Fajas, L., C. Paul, O. Zugasti, L. Le Cam, J. Polanowska, E. Fabbrizio, R. Medema, M.L. Vignais, and C. Sardet. 2000. pRB binds to and modulates the transrepressing activity of the E1A-regulated transcription factor p120E4F. *Proc Natl Acad Sci U S A* 97:7738-7743.
- Fenton, S.L., A. Dallol, A. Agathangelou, L. Hesson, J. Ahmed-Choudhury, S. Baksh, C. Sardet, R. Dammann, J.D. Minna, J. Downward, E.R. Maher, and F. Latif. 2004. Identification of the E1A-regulated transcription factor p120 E4F as an interacting partner of the RASSF1A candidate tumor suppressor gene. *Cancer Res* 64:102-107.
- Fernandes, E.R., J.Y. Zhang, and R.J. Rooney. 1998. Adenovirus E1A-regulated transcription factor p120E4F inhibits cell growth and induces the stabilization of the cdk inhibitor p21WAF1. *Mol Cell Biol* 18:459-467.
- Guerra, C., N. Mijimolle, A. Dhawahir, P. Dubus, M. Barradas, M. Serrano, V. Campuzano, and M. Barbacid. 2003. Tumor induction by an endogenous K-ras oncogene is highly dependent on cellular context. *Cancer Cell*. 4:111-120.
- Huang, P., L. Feng, E.A. Oldham, M.J. Keating, and W. Plunkett. 2000. Superoxide dismutase as a target for the selective killing of cancer cells. *Nature* 407:390-395.10.1038/35030140.

- Huang, Q., Y.T. Wu, H.L. Tan, C.N. Ong, and H.M. Shen. 2009. A novel function of poly(ADP-ribose) polymerase-1 in modulation of autophagy and necrosis under oxidative stress. *Cell Death Differ* 16:264-277.cdd2008151 [pii] 10.1038/cdd.2008.151.
- Kamijo, T., F. Zindy, M.F. Roussel, D.E. Quelle, J.R. Downing, R.A. Ashmun, G. Grosveld, and C.J. Sherr. 1997. Tumor suppression at the mouse INK4a locus mediated by the alternative reading frame product p19ARF. *Cell* 91:649-659.S0092-8674(00)80452-3 [pii].
- Khoo, C.M., D.R. Carrasco, M.W. Bosenberg, J.H. Paik, and R.A. Depinho. 2007. Ink4a/Arf tumor suppressor does not modulate the degenerative conditions or tumor spectrum of the telomerase-deficient mouse. *Proc Natl Acad Sci U S A* 104:3931-3936.0700093104 [pii] 10.1073/pnas.0700093104.
- Kim, W.Y., and N.E. Sharpless. 2006. The regulation of INK4/ARF in cancer and aging. *Cell* 127:265-275.S0092-8674(06)01284-0 [pii] 10.1016/j.cell.2006.10.003.
- Koopman, W.J., L.G. Nijtmans, C.E. Dieteren, P. Roestenberg, F. Valsecchi, J.A. Smeitink, and P.H. Willems. 2010. Mammalian mitochondrial complex I: biogenesis, regulation, and reactive oxygen species generation. *Antioxid Redox Signal* 12:1431-1470.10.1089/ars.2009.2743.
- Lacroix, M., J. Caramel, P. Goguet-Rubio, L.K. Linares, S. Estrach, E. Hatchi, G. Rodier, G. Lledo, C. de Bettignies, A. Thepot, C. Deraison, K. Chebli, A. Hovnanian, P. Hainaut, P. Dubus, C. Sardet, and L. Le Cam. 2010. Transcription factor E4F1 is essential for epidermal stem cell maintenance and skin homeostasis. *Proc Natl Acad Sci U S A* 107:21076-21081.1010167107 [pii] 10.1073/pnas.1010167107.

- Le Cam, L., M. Lacroix, M.A. Ciemerych, C. Sardet, and P. Sicinski. 2004. The E4F protein is required for mitotic progression during embryonic cell cycles. *Mol Cell Biol* 24:6467-6475.
- Le Cam, L., L.K. Linares, C. Paul, E. Julien, M. Lacroix, E. Hatchi, R. Triboulet, G. Bossis, A. Shmueli, M.S. Rodriguez, O. Coux, and C. Sardet. 2006. E4F1 is an atypical ubiquitin ligase that modulates p53 effector functions independently of degradation. *Cell*. 127:775-788.
- Lee, K.A., and M.R. Green. 1987. A cellular transcription factor E4F1 interacts with an E1a-inducible enhancer and mediates constitutive enhancer function in vitro. *Embo J* 6:1345-1353.
- Lee, K.A., T.Y. Hai, L. SivaRaman, B. Thimmappaya, H.C. Hurst, N.C. Jones, and M.R. Green. 1987. A cellular protein, activating transcription factor, activates transcription of multiple E1A-inducible adenovirus early promoters. *Proc Natl Acad Sci U S A* 84:8355-8359.
- Levine, B., and G. Kroemer. 2008. Autophagy in the pathogenesis of disease. *Cell* 132:27-42.S0092-8674(07)01685-6 [pii] 10.1016/j.cell.2007.12.018.
- Lund, A.H., G. Turner, A. Trubetskoy, E. Verhoeven, E. Wientjens, D. Hulsman, R. Russell, R.A. DePinho, J. Lenz, and M. van Lohuizen. 2002. Genome-wide retroviral insertional tagging of genes involved in cancer in Cdkn2a-deficient mice. *Nat Genet* 32:160-165.10.1038/ng956 ng956 [pii].
- Martin-Caballero, J., J.M. Flores, P. Garcia-Palencia, and M. Serrano. 2001. Tumor susceptibility of p21(Waf1/Cip1)-deficient mice. *Cancer Res* 61:6234-6238.
- Mizushima, N. 2009. Physiological functions of autophagy. *Curr Top Microbiol Immunol* 335:71-84.10.1007/978-3-642-00302-8_3.

- Nogueira, V., Y. Park, C.C. Chen, P.Z. Xu, M.L. Chen, I. Tonic, T. Unterman, and N. Hay. 2008. Akt determines replicative senescence and oxidative or oncogenic premature senescence and sensitizes cells to oxidative apoptosis. *Cancer Cell* 14:458-470.S1535-6108(08)00370-X [pii] 10.1016/j.ccr.2008.11.003.
- Nojima, J., K. Kanomata, Y. Takada, T. Fukuda, S. Kokabu, S. Ohte, T. Takada, T. Tsukui, T.S. Yamamoto, H. Sasanuma, K. Yoneyama, N. Ueno, Y. Okazaki, R. Kamijo, T. Yoda, and T. Katagiri. Dual roles of smad proteins in the conversion from myoblasts to osteoblastic cells by bone morphogenetic proteins. *J Biol Chem* 285:15577-15586.M109.028019 [pii] 10.1074/jbc.M109.028019.
- Paul, C., M. Lacroix, I. Iankova, E. Julien, B.W. Schafer, C. Labalette, Y. Wei, A. Le Cam, L. Le Cam, and C. Sardet. 2006. The LIM-only protein FHL2 is a negative regulator of E4F1. *Oncogene*. 25:5475-5484. Epub 2006 May 5471.
- Quelle, D.E., F. Zindy, R.A. Ashmun, and C.J. Sherr. 1995. Alternative reading frames of the INK4a tumor suppressor gene encode two unrelated proteins capable of inducing cell cycle arrest. *Cell* 83:993-1000.0092-8674(95)90214-7 [pii].
- Raychaudhuri, P., R. Rooney, and J.R. Nevins. 1987. Identification of an E1A-inducible cellular factor that interacts with regulatory sequences within the adenovirus E4 promoter. *Embo J* 6:4073-4081.
- Rizos, H., E. Diefenbach, P. Badhwar, S. Woodruff, T.M. Becker, R.J. Rooney, and R.F. Kefford. 2003. Association of p14ARF with the p120E4F transcriptional repressor enhances cell cycle inhibition. *J Biol Chem* 278:4981-4989.
- Rooney, R.J. 2001. Cell cycle attenuation by p120E4F is accompanied by increased mitotic dysfunction. *Cell Growth Differ* 12:505-516.

- Rui, E., P.R. Moura, K.A. Goncalves, R.J. Rooney, and J. Kobarg. 2006. Interaction of the hepatitis B virus protein HBx with the human transcription regulatory protein p120E4F in vitro. *Virus Res.* 115:31-42. Epub 2005 Aug 2002.
- Sandy, P., M. Gostissa, V. Fogal, L.D. Cecco, K. Szalay, R.J. Rooney, C. Schneider, and G. Del Sal. 2000. p53 is involved in the p120E4F-mediated growth arrest. *Oncogene* 19:188-199.
- Serrano, M., H. Lee, L. Chin, C. Cordon-Cardo, D. Beach, and R.A. DePinho. 1996. Role of the INK4a locus in tumor suppression and cell mortality. *Cell.* 85:27-37.
- Sharpless, N.E., N. Bardeesy, K.H. Lee, D. Carrasco, D.H. Castrillon, A.J. Aguirre, E.A. Wu, J.W. Horner, and R.A. DePinho. 2001. Loss of p16Ink4a with retention of p19Arf predisposes mice to tumorigenesis. *Nature* 413:86-91.10.1038/35092592 .
- Struthers, L., R. Patel, J. Clark, and S. Thomas. 1998. Direct detection of 8-oxodeoxyguanosine and 8-oxoguanine by avidin and its analogues. *Anal Biochem* 255:20-31.S0003-2697(97)92354-X [pii] 10.1006/abio.1997.2354.
- Sundstrom, C., and K. Nilsson. 1976. Establishment and characterization of a human histiocytic lymphoma cell line (U-937). *Int J Cancer* 17:565-577.
- Tasdemir, E., M.C. Maiuri, L. Galluzzi, I. Vitale, M. Djavaheri-Mergny, M. D'Amelio, A. Criollo, E. Morselli, C. Zhu, F. Harper, U. Nannmark, C. Samara, P. Pinton, J.M. Vicencio, R. Carnuccio, U.M. Moll, F. Madeo, P. Paterlini-Brechot, R. Rizzuto, G. Szabadkai, G. Pierron, K. Blomgren, N. Tavernarakis, P. Codogno, F. Cecconi, and G. Kroemer. 2008. Regulation of autophagy by cytoplasmic p53. *Nat Cell Biol.* 10:676-687. Epub 2008 May 2004.
- Tessari, M.A., M. Gostissa, S. Altamura, R. Sgarra, A. Rustighi, C. Salvagno, G. Caretti, C. Imbriano, R. Mantovani, G. Del Sal, V. Giancotti, and G. Manfioletti. 2003.

- Transcriptional activation of the cyclin A gene by the architectural transcription factor HMGA2. *Mol Cell Biol* 23:9104-9116.
- Trachootham, D., H. Zhang, W. Zhang, L. Feng, M. Du, Y. Zhou, Z. Chen, H. Pelicano, W. Plunkett, W.G. Wierda, M.J. Keating, and P. Huang. 2008. Effective elimination of fludarabine-resistant CLL cells by PEITC through a redox-mediated mechanism. *Blood* 112:1912-1922.blood-2008-04-149815 [pii] 10.1182/blood-2008-04-149815.
- Trachootham, D., Y. Zhou, H. Zhang, Y. Demizu, Z. Chen, H. Pelicano, P.J. Chiao, G. Achanta, R.B. Arlinghaus, J. Liu, and P. Huang. 2006. Selective killing of oncogenically transformed cells through a ROS-mediated mechanism by beta-phenylethyl isothiocyanate. *Cancer Cell* 10:241-252.S1535-6108(06)00250-9 [pii] 10.1016/j.ccr.2006.08.009.
- Valko, M., D. Leibfritz, J. Moncol, M.T. Cronin, M. Mazur, and J. Telser. 2007. Free radicals and antioxidants in normal physiological functions and human disease. *Int J Biochem Cell Biol* 39:44-84.S1357-2725(06)00219-6 [pii] 10.1016/j.biocel.2006.07.001.
- Vousden, K.H., and K.M. Ryan. 2009. p53 and metabolism. *Nat Rev Cancer* 9:691-700.nrc2715 [pii] 10.1038/nrc2715.
- Xu, Y., S.O. Kim, Y. Li, and J. Han. 2006. Autophagy contributes to caspase-independent macrophage cell death. *J Biol Chem* 281:19179-19187.M513377200 [pii] 10.1074/jbc.M513377200.
- Zhu, H., L. Zhang, K. Itoh, M. Yamamoto, D. Ross, M.A. Trush, J.L. Zweier, and Y. Li. 2006. Nrf2 controls bone marrow stromal cell susceptibility to oxidative and electrophilic stress. *Free Radic Biol Med* 41:132-143.S0891-5849(06)00214-0 [pii] 10.1016/j.freeradbiomed.2006.03.020.

Figure legends

Figure 1. Development of a mouse model of HS harboring *E4F1* conditional KO allele.

(A) Schematic representation of the different *E4F1 flox*, *RERT* KI and *Ink4a/Arf* null alleles.

(B) 4OHT administration results in efficient Cre-mediated *E4F1* inactivation. RT-qPCR (upper and lower panels, mean \pm SD, n=3) and immunoblotting (middle panels) analyses of *E4F1* expression levels in tissues isolated from *E4F1*^{+/flox} or *E4F1*^{-/flox}; *RERT*^{KI/KI} mice after repeated administration of 4OHT. RT-qPCR products were loaded on agarose gels (upper panels) after real time PCR amplification to verify fragment size and purity of amplicons. *HPRT* mRNA and GAPDH protein were used to normalize RT-qPCR and immunoblots, respectively. BM cells represent total bone marrow cells. BM Lin- cells represent a fraction of purified BM cells enriched in hematopoietic stem and progenitor cells that were negatively selected for expression of lineage specific markers (CD3, B220, Ter119, Gr-1, Mac1).

(C) Microphotographs of representative H&E-stained histological lung and liver sections from transplanted mice. Dashed lines indicate the edge of the infiltrating HS. Inserts show high magnification images of HS cells exhibiting large eosinophilic cytoplasm and reniform nucleus. Scale bar: 50 μ m.

(D) Immunophenotypical analysis of HS. Representative tumors observed in lung and liver were analyzed by immunohistochemistry (IHC) using antibodies for the proliferation marker Ki67 (DAB, brown staining) and the histiocytic marker F4/80 (VIP, dark purple staining), as indicated. Scale bar: 50 μ m.

Figure 2. *E4F1* inactivation results in decreased tumor development and increased lifespan.

A) Kaplan-Meier survival curve of transplanted *E4F1* CT; *Ink4a/Arf* WT (n=8), *E4F1* KO; *Ink4a/Arf* WT (n=16), *E4F1* CT; *Ink4a/Arf* KO (n=24), *E4F1* KO; *Ink4a/Arf* KO (n=30) mice, as indicated. Black arrow indicates the first 4OHT administration. Statistically significant differences for pairwise comparison were evaluated by a log-Rank test. *, p=0.005; NS, non statistically significant.

(B) IHC analyses of lung sections of *E4F1* CT or KO; *Ink4a/Arf* KO mice stained with an antibody for the Mac2 histiocytic specific marker. Representative microphotographs at low and high magnification are shown. Scale bar: 1mm (low mag.) and 100 μ m (high mag.).

(C) Spleen weight of *E4F1* CT or KO; *Ink4a/Arf* KO animals. Microphotograph of spleen from a representative *E4F1* CT or KO; *Ink4a/Arf* KO mouse. Untransplanted tumor free mice were used as controls (median \pm SD, n=17 for each group).

Figure 3. *E4F1* inactivation results in cell death and tumor regression in established HS.

(A and B) 18 F-FDG based PET-scan analyses were performed on individual *E4F1* CT or KO; *Ink4a/Arf* KO mice before (upper panels) or 2 weeks after (lower panels) repeated administrations of 4OHT (n=4 for each group). (A) Representative images showing HS regression in spleen (red dashed line) and liver (white dashed line) in *E4F1* KO; *Ink4a/Arf* KO mouse, in contrast to HS progression in *E4F1* CT; *Ink4a/Arf* KO mouse. The color code indicates radioactivity intensity (arbitrary units) representing 18 F-FDG uptake. Note that strong PET signal in heart and pectoral muscles precluded analysis of tumor progression in lungs. (B) Quantitative analysis of PET imaging performed on spleen and liver (Fold change representing the ratio between PET signal after (D15) and before (D0) 4OHT administration

to *E4F1* CT or KO; *Ink4a/Arf* KO mice (median \pm SD of 4 animals for each genotype). (C) Representative microphotograph of TUNEL staining performed on lung tissue sections prepared from *E4F1* CT or KO; *Ink4a/Arf* KO mice 15 days after 4OHT administration. Sections were colabelled with TUNEL, Mac2 and DAPI, as indicated. Merge images (Mac2-Red / TUNEL-Green) are shown at higher magnification. Scale bar: 50 μ m

Figure 4. *E4F1* inactivation induces massive cell death of HS cells

(A) *E4F1* inactivation in HS cells results in decreased number of viable cells, 3 days after 4OHT addition in the culture medium (mean \pm SD, n=6). Immunoblot analyses (right panels) of *E4F1* and GAPDH (loading control) expression levels in *E4F1* CT and KO HS cells.

(B) Proliferation rate and mitotic index are not altered in *E4F1* KO HS cells. The percentage of EdU (left panel) or phospho-histone H3 (S10) (PHH3) (right panel) positive cells were evaluated by flow cytometry (mean \pm SD, n=3). Nocodazole treatment (Noco) of *E4F1* CT HS cells was used as a control for PHH3 staining.

(C) *E4F1* inactivation induces massive cell death. Representative microphotographs (top panels) and flow cytometry analyses of annexin positive cells (lower panels) in *E4F1* CT and KO HS cells (numbers indicate the mean \pm SD of n=7).

(D) *E4F1* inactivation abrogates colony formation in soft agar. Colony numbers were evaluated after 3 weeks of culture. Quantitative evaluation of total number of colonies formed by *E4F1* CT and KO HS cells (mean \pm SD, n=3)

Figure 5. *E4F1* inactivation in HS cells results in autophagic cell death.

(A) Representative microphotographs of electron microscopy analyses (X6000 magnification) showing formation of autophagic vacuoles in *E4F1* KO HS cells. Inserts correspond to a

X20000 magnification of the same cells showing apparition of double membraned cytoplasmic vacuoles containing dark degradation products in *E4F1* KO HS cells (white arrows). Scale bars: 500 nm.

(B) Quantitative immunoblot analyses of LC3 expression in *E4F1* HS cells showing increased conversion of LC3-I to LC3-II upon *E4F1* inactivation that is rescued by the autophagy inhibitor 3MA. Actin was used as a loading control. Upper panels show representative immunoblots. Lower panel represents the quantitative analyses of LC3-II levels normalized to actin levels (mean \pm SD, n=3).

(C) *E4F1* inactivation results in increased formation of autophagolysosomes. Representative microphotograph of *E4F1* HS cells stained with anti-LC3 antibody and DAPI and visualized by fluorescence microscopy. Scale bar: 10 μ m

(D) Formation of acidic vesicular organelles (AVO) in *E4F1* KO HS cells was visualized by fluorescence microscopy after staining with the lysosomal specific dye acridine orange (AO) and DAPI. Scale bar: 10 μ m

(E) *E4F1* inactivation results in increased cell death that is abrogated by 3MA treatment. Percentage of annexin positive cells measured in *E4F1* HS cells by flow cytometry upon annexin staining (mean \pm SD, n=3).

Figure 6. ***E4F1* inactivation results in mitochondrial defects and increased ROS levels**

(A) Flow cytometry analyses of ROS levels measured by the DCFDA (upper left panel), Oxyburst (upper right panel) and the mitochondrial specific (lower panels) MitoSOX probes in *E4F1* CT and KO HS cells, as indicated. Histograms represent quantitative data showing fold increase of time dependent changes in mean fluorescence intensity of MitoSOX measured by flow cytometry (mean \pm SD, n=3).

(B) *E4F1* inactivation increases mitochondrial O₂ consumption rate (OCR). Representative experiment measuring OCR corresponding to basal respiration, oligomycin-sensitive OCR, and maximal respiration (upon injection with the uncoupling agent FCCP and rotenone) in *E4F1* CT and KO HS cells, as indicated. Values were normalized to total protein levels. Vertical bars indicate the time of injection of the indicated compound.

(C) *E4F1* inactivation decreases total ATP levels. Histograms represent total ATP levels in *E4F1* CT and KO HS cells, 3 days after 4OHT addition (mean \pm SD, n=3).

(D) Increased ROS levels in *E4F1* KO HS cells result in increased genomic DNA oxidation. 8-OHdG levels were evaluated by fluorescence microscopy in presence or absence of the superoxide anion scavenger Tiron, using a binding assay based on avidin-conjugated FITC. Representative images of 3 independent experiments are shown. Scale bar: 10 μ m

(E) Quantitative immunoblot analyses of LC3 expression in total protein extracts prepared from *E4F1* CT and KO HS cells treated with vehicle, Tiron, or D3T, as indicated. LC3-II levels were normalized to actin levels (mean \pm SD, n=3).

Figure 7. ROS scavengers rescue cell death occurring in *E4F1* KO HS cells

(A) Number of viable cells assessed in absence or presence of the ROS scavengers Tiron or NAC, or upon addition of D3T in *E4F1* KO or CT HS cells, as indicated (mean \pm SD, n=3).

(B and C) NAC administration rescues cell death *in vivo* in *E4F1* KO; *Ink4a/Arf* KO mice. Representative microphotograph of TUNEL staining performed on liver tissue sections prepared from vehicle (B) or NAC (C) -treated *E4F1* CT or KO; *Ink4a/Arf* KO mice, 15 days after 4OHT administration. Sections were colabelled with TUNEL, Mac2 and DAPI as indicated. Merge images (Mac2-Red/ TUNEL-Green) are shown at higher magnification. Scale bar: 50 μ m

Figure 8. *E4F1* inactivation does not result in mitochondrial defects, increased ROS levels or increased cell death in normal primary macrophages.

Primary macrophages were purified from the intra-peritoneal cavity of age-matched *E4F1* CT or KO animals. *E4F1* inactivation was induced *ex-vivo* by addition of 4OHT in the culture medium. Analyses were performed between 4 and 5 days upon 4OHT addition.

(A) Immunoblot analysis showing E4F1 depletion in primary macrophages. GAPDH was used as a loading control.

(B) Flow cytometry analysis of intracellular ROS levels (DCFDA) in *E4F1* CT and KO primary macrophages.

(C) *E4F1* inactivation in primary macrophages does not induce cell death. *E4F1* CT or KO primary macrophages were analyzed by flow cytometry upon annexin staining.

(D) *E4F1* inactivation in *E4F1* CT or KO primary macrophages does not induce mitochondrial defects. OCR was measured as described in Fig. 6.

Data are representative of 4 independent experiments.

Figure 9. E4F1 is overexpressed in human AML samples and its depletion induces mitochondrial defects, increased ROS levels and cell death in human myeloid leukemic cell lines.

(A) Western blot analysis showing efficient depletion of E4F1 in human histiocytic sarcoma U937, erythroleukemic HEL, promyelocytic leukemia HL60, and acute monocytic leukemia THP1 cell lines, transduced with lentiviruses encoding independent ShRNAs (shE4F1 #1 and #2) directed against human E4F1, or a control irrelevant ShRNA (shCt).

(B) ShRNA-mediated depletion of E4F1 in human leukemic cell lines induces increased ROS levels. Representative flow cytometry analyses of ROS levels (DFCDA) upon shRNA-mediated depletion of E4F1 in U937, HEL, HL60 and THP1 cell lines.

(C) Increased O₂ consumption in human HEL, HL60 myeloid leukemic cell lines upon treatment with Ct or E4F1 shRNA, as indicated. O₂ consumption was measured using a Clark-type O₂ electrode chamber.

(D) Flow cytometry analyses of annexin positive cells in human myeloid leukemic cell lines upon treatment with Ct or E4F1 shRNAs, as indicated. Histograms represent the mean \pm SD, n=3.

(E) E4F1 protein levels in human acute myeloid leukemia (AML) bone marrow samples. E4F1 and actin (loading control) protein expression levels were evaluated by quantitative immunoblotting on total protein extracts prepared from bone marrow samples from adult AML patients. Histograms represent the ratio between E4F1 and actin levels of individual patients. The dotted line represents the mean value of this ratio obtained with 3 normal bone marrow samples. Percentage of myeloid leukemic blasts in each sample was evaluated to avoid potential biases based on heterogeneity of the AML bone marrow sample tested.

Supplementary Materials and methods

Evaluation of recombination efficiency

E4F1 recombination was assessed by immunoblotting or by quantitative PCR analysis on genomic DNA using primers specific for the *E4F1* locus, as described in Fig. S1A: primer A: 5'-GGCTGCTGCGTGGATTTC, B: 5'-GCTAGGTAGGGTAGGAGGCTGTCT, C: 5'-TTCGGTATAGTGTGAGG, D: 5'-AGGGGCTGGGCTACAATGG.

Genotyping

E4F1 flox; *RERT* mice were genotyped by PCR on tail genomic DNA using the following primers: i) *E4F1* WT (*E4F1*⁺) and conditional knock-out flox alleles (*E4F1* flox): 5'-CCTTGAGCACGGAGGAGAGC-3' and 5'-GCCCTAGCCTGCTC-TGCCATC-3'. ii) *E4F1* constitutive KO allele (*E4F1*⁻): 5'-CACTGCCTTGGAGGACTTTG-3' and 5'-CCTCTGTTCCACA-TACTTTCATTC-3'. iii) WT and KI *RERT* alleles: 5'-GTCAGTACACATACAGACTT-3', 5'-TGAGCGAACAGGGCGAA-3' and 5'-TCCATGGAGCACCCAGTGAA-3', iv) *Ink4a/Arf* alleles: wild type 5'-ATGATGATGGGCAACGTTC-3' and 5'-CAAATATCGCACGATGTC-3'; knock-out: 5'-CTATCAGGACATAGCGTTGG-3' and 5'-AGTGAGAGTTTGGGGACAGAG-3'.

Immunoblotting

Antibodies used for western blotting were rabbit monoclonal anti p-Akt (S473) and rabbit polyclonal anti-total Akt (Cell Signaling Technology), anti-PTEN (A2B1, Santa Cruz), and GAPDH (Santa Cruz). HRP-conjugated anti-goat was used for secondary antibodies and purchased from GE healthcare.

Lentiviral particles productions and infections

For ShRNA mediated depletion of murine p53 in *E4F1* HS cells, we used the following constructs: pLKO1 encoding an shRNA directed against murine p53 (Sigma mission shRNA clone 1526s1c1), or an irrelevant shRNA (shCt, clone shc002). 48 hrs after transfection, viral particles were harvested in the supernatant and added in the culture medium of *E4F1* HS cells in presence of polybrene (8 μ g/ml final). Immunoblotting on total protein extracts was performed to confirm p53 depletion. ROS levels and cell death were evaluated 5 to 7 days after the infection by flow cytometry upon incubation with DCFDA or annexin/PI.

Legends of supplementary figures

Figure S1. Experimental model based on transplantation of HSC harboring *E4FI* conditional KO allele.

(A) Schematic representation of the modified *E4FI flox* allele before and after Cre-mediated recombination (left panel). Recombination efficiency of *E4FI flox* allele was verified by quantitative PCR (Q-PCR) with the indicated sets of primers (arrows) on genomic DNA isolated from several hematopoietic tissues, including spleen, blood and bone marrow of *E4FI^{-/flox}; RERT^{KI/KI}* adult mice after topical applications of 4OHT (right panel). Genomic DNA extracted from the spleen of a non-treated mouse was used as a control. Q-PCR products were loaded on agarose gels after PCR amplification. Note that primers pair A/B generates a PCR amplicon only after Cre-mediated recombination. Normalization for equal amount of genomic DNA in those assays was controlled with primers (C/D) located in the non-recombined region of the *E4FI* locus.

(B) Schematic representation of the experimental setting. Experimental groups were generated by transplantation of HSC donor cells, isolated from fetal liver of Ly5.2 *E4FI* CT or KO; *Ink4a/Arf* KO E14.5 embryos. 10 weeks after transplantation, reconstituted animals were treated by topical applications of 4OHT (2mg/animal/application, 3 applications). 4OHT administrations were repeated every 4 weeks. Tumor development in living animals was followed by palpation and flow cytometry analyses on peripheral blood samples every 4 weeks.

(C) Evaluation of reconstitution efficiency in transplanted mice. Percentages of donor (Ly5.2 positive) and host cells (Ly5.1 positive) were evaluated by multiparameter flow cytometry analyses in the peripheral blood from transplanted animals. Data from a representative mouse is shown. Numbers in each quadrant indicate the mean value \pm SD of 110 animals analyzed.

(D) Representative IHC analyses of serial lung sections from *E4F1* CT; *Ink4a/Arf* KO animal stained with anti-F4/80 (histiocyte), -CD3 (T-lymphocyte) or -Pax5 (B-lymphocyte) antibodies. Revelation was performed using VIP (dark purple) as a substrate. Sections were counterstained with hematoxylin. Note that HS are negative for the CD3 and Pax5 lymphoid markers. Representative microphotographs at low and high magnification are shown.

(E) Tumor spectrum in genetically matched untransplanted *E4F1* flox; *RERT*^{K1/K1}; *Ink4a/Arf* KO donor mice and Ly5.1 recipient mice transplanted with *E4F1* flox; *RERT*^{K1/K1}; *Ink4a/Arf* KO foetal HSC. Note that genetically matched donor mice develop preferentially lymphomas and sarcomas, as previously described (Serrano et al., 1996).

(F) HS progression was assessed by evaluating the proportion of circulating F4/80+ HS cells in peripheral blood of transplanted mice. Representative multiparameter flow cytometry analysis performed on peripheral blood of *E4F1* CT; *Ink4a/Arf* KO mice, showing increased number of F4/80+ HS cells between 10 and 20 weeks after transplantation. *E4F1* CT; *Ink4a/Arf* WT mice were used as controls.

Figure S2. *E4F1* inactivation in HS results in decreased tumor development and tumor regression in established HS.

(A) Control PET imaging of non transplanted control mouse showing high PET signal in heart, pectoral muscles and head that precluded the analysis of HS progression in lungs.

(B) IHC analyses of lung sections stained with the F4/80 histiocyte specific marker showing decreased tumor development in *E4F1* KO; *Ink4a/Arf* KO mice when compared to their *E4F1* CT; *Ink4a/Arf* KO control mice. Representative microphotographs at low and high magnification are shown. Scale bar: 1mm (low mag.) and 100µm (high mag.).

(C) Quantitative analysis of PET imaging performed on spleen and liver, before (D0) and after (D15) 4OHT administration to *E4F1* CT or KO; *Ink4a/Arf* KO mice (median \pm SD of 4 animals for each genotype).

Figure S3. Functional perturbation of the oncogenic PI3K pathway in murine HS.

(A) Immunoblot analyses of E4F1, PTEN, and GAPDH (loading control) protein levels. Note that PTEN is still expressed in *E4F1* HS cells.

(B) Deregulation of the PI3K/AKT pathway in murine *E4F1 flox* HS cells. Quantitative immunoblotting of total and Phospho-Ser473-AKT on total protein extracts from HS cell lines and primary macrophages, as indicated. GAPDH immunoblot was performed as a loading control. Quantification of the P-Akt / GAPDH ratio (upper panel).

Figure S4. Immunophenotypical characterization of *E4F1* HS cell lines derived from primary tumors.

(A) Representative microphotograph and immunofluorescence images of *E4F1* HS cell line stained with anti-F4/80 and anti-Mac2 antibodies.

(B) Representative multiparameter flow cytometry analysis of one *E4F1* HS cell line showing F4/80 and Mac2 expression patterns.

(C) E4F1 and GAPDH immunoblots (left panels) performed on protein extracts from *E4F1*^{+/flox} HS cell line, in presence or absence of 4OHT. Evaluation of cell proliferation and viability of *E4F1*^{+/flox} HS cell line, in presence or absence of 4OHT.

Figure S5. *E4F1* inactivation results in autophagic cell death with minor contribution of apoptosis. Increased ROS levels trigger cell death in *E4F1* KO HS cells

(A) Flow cytometry analysis of annexin stained *E4F1 CT* and *KO* HS cell lines after 4 days of culture in absence or presence of the caspase inhibitor z-VAD.

(B) Histograms represent flow cytometry analyses of annexin positive cells in absence or presence of Tiron or D3T, as indicated (mean \pm SD, n=3).

Figure S6. *E4F1* inactivation induces mitochondrial defects, increased ROS levels, and a cellular anti-oxidant response.

(A) Flow cytometry analyses (DFCDA) of ROS levels in *E4F1 CT* or *KO* HS cells, in presence or absence of 3MA, as indicated.

(B) Representative immunofluorescence images showing increased mitochondrial superoxide anion levels in *E4F1 KO* HS cells visualized by the MitoSOX probe. Scale bar: 25 μ m

(C-G) *E4F1* inactivation induces a cellular anti-oxidant response in HS cells. Representative immunofluorescence images showing increased protein expression of the anti-oxidant proteins heme oxygenase 1 (HO1) (C), NAD(P)H dehydrogenase quinone 1 (NQO1) (D), and catalase (E) in *E4F1 KO* HS cells, as indicated. Scale bar: 25 μ m. (F) Immunoblot analyses showing increased expression of the anti-oxidant proteins NRF2, catalase, HO1 in *E4F1 KO* HS cells, as indicated. Actin was used as a loading control.

(G) *E4F1* inactivation results in increased O₂ consumption. O₂ consumption was measured using a temperature-regulated Clark-type O₂ electrode chamber in murine *E4F1* HS cells (mean \pm SD, n=3).

(H) Flow cytometry analyses (DFCDA) of ROS levels in *E4F1 CT* or *KO* HS cells (left panel), in presence or absence of D3T, as indicated. Histograms represent quantitative analyses (mean \pm SD, n=3).

Figure S7. ROS production and autophagic cell death does not result from p53 activation.

(A) p53 and GAPDH immunoblots performed on protein extracts from one representative *E4F1* HS cell line transduced with lentiviruses encoding a shRNA targeting murine p53 (Shp53), or a control ShRNA (shCt). Protein extracts prepared from p53 null Mefs were used as a control.

(B) Flow cytometry analyses (DFCDA) of ROS levels in *E4F1* CT or KO HS cells transduced with lentiviruses encoding a shRNA targeting murine p53, or a control shRNA (shCt).

(C) Flow cytometry analyses of annexin positive cells in *E4F1* CT and KO HS cells transduced with lentiviruses encoding a shRNA targeting murine p53, or a control ShRNA (shCt).

Figure S8. E4F1 protein is overexpressed in murine HS cells and a large subset of human AML bone marrow samples

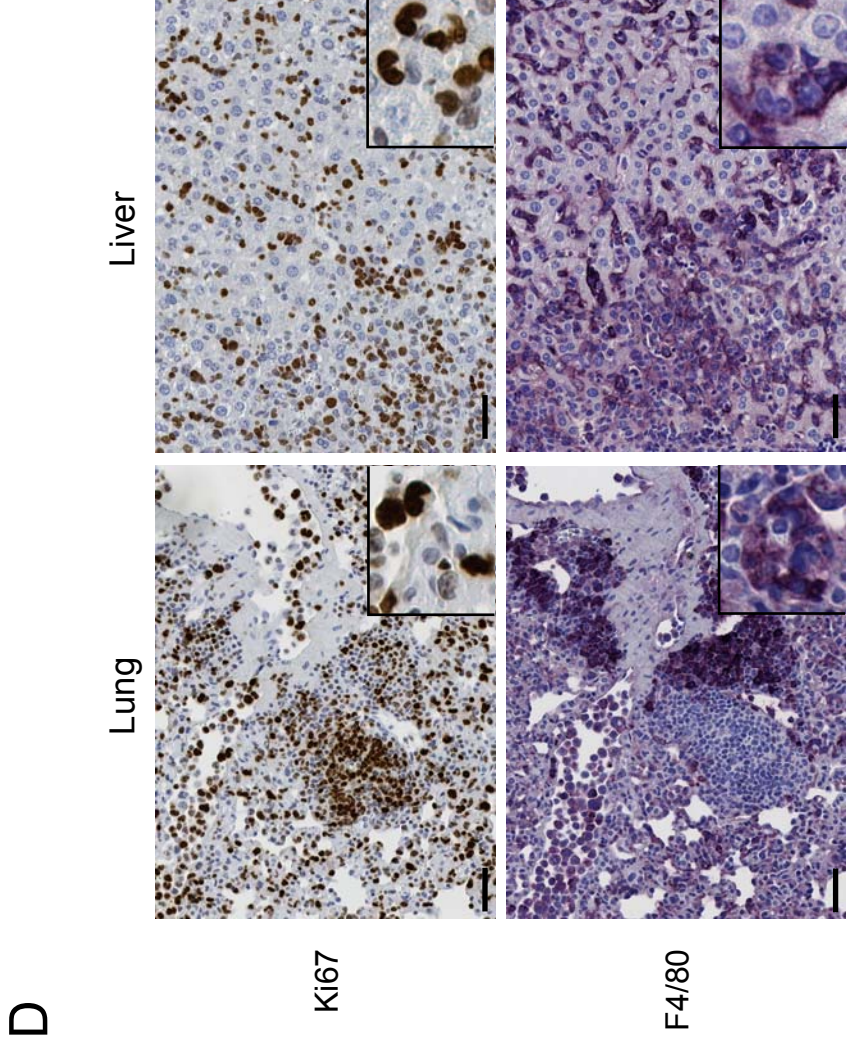
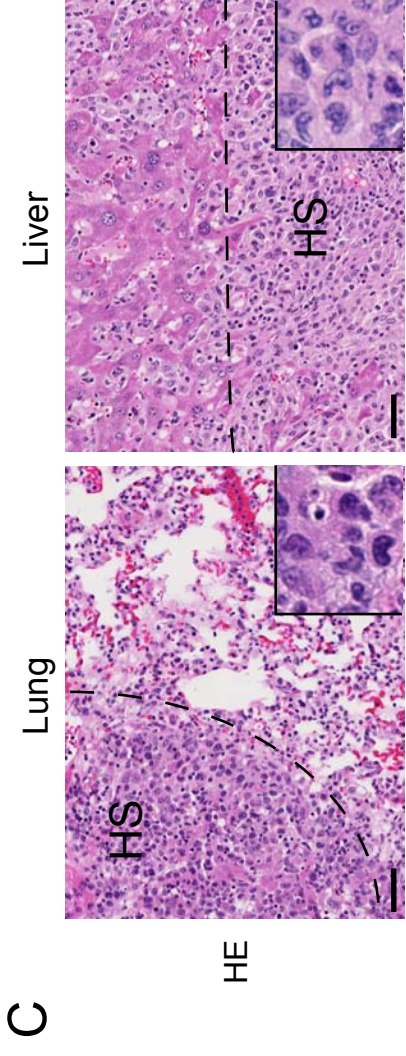
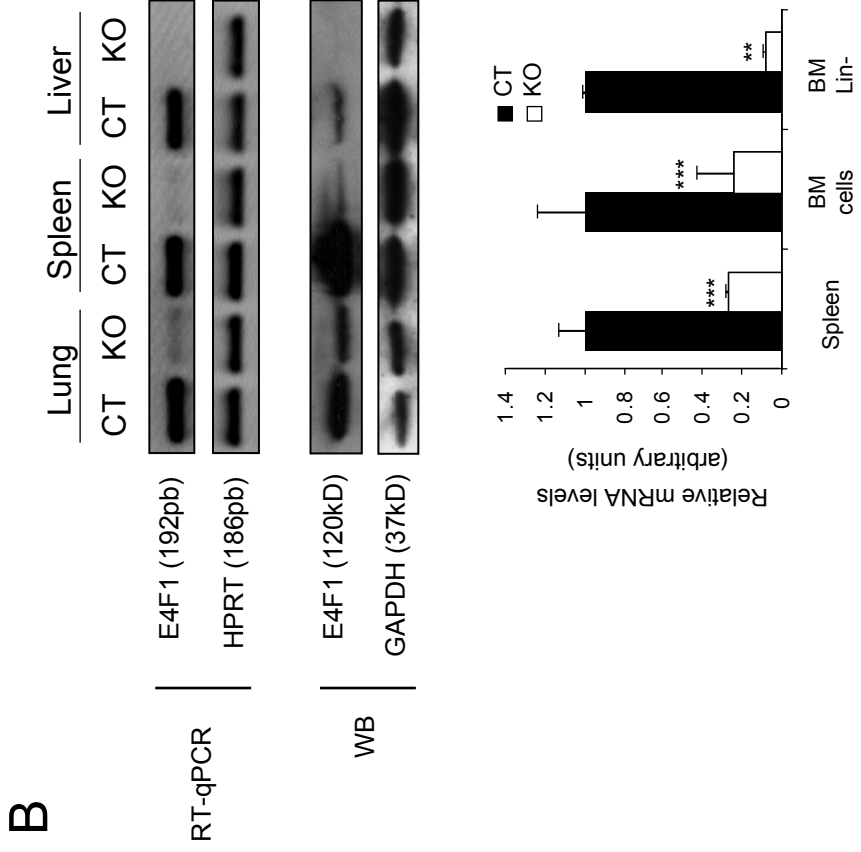
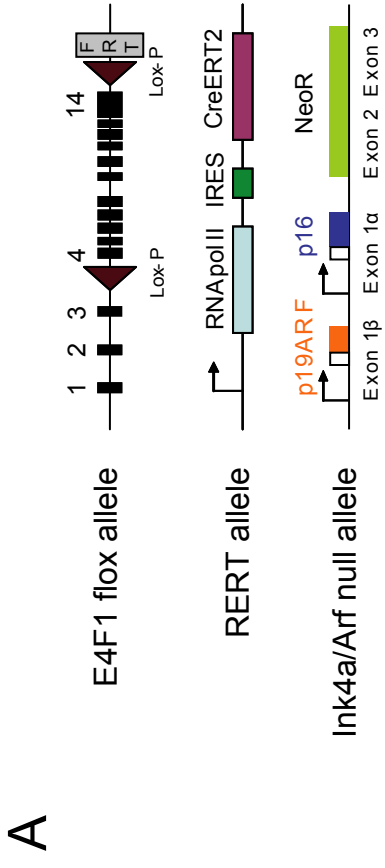
(A) Semi-quantitative enhanced chemiluminescence (ECL) -based immunoblot analyses showing increased protein expression of E4F1 in HS cells compared to normal primary macrophages, 5 days after 4OHT addition, as indicated. Short and long exposures of the same anti-E4F1 immunoblot are shown. GAPDH was used as a loading control. Note that the remaining E4F1-signal in *E4F1* KO HS cells is the consequence of massive cell death and high selective pressure for unrecombined cells when analyses are performed later than 4 days after 4OHT addition.

(B) RT-qPCR analyses of E4F1 mRNA expression level in *E4F1* in HS cells compared to normal primary macrophages (mean \pm SD, n=3).

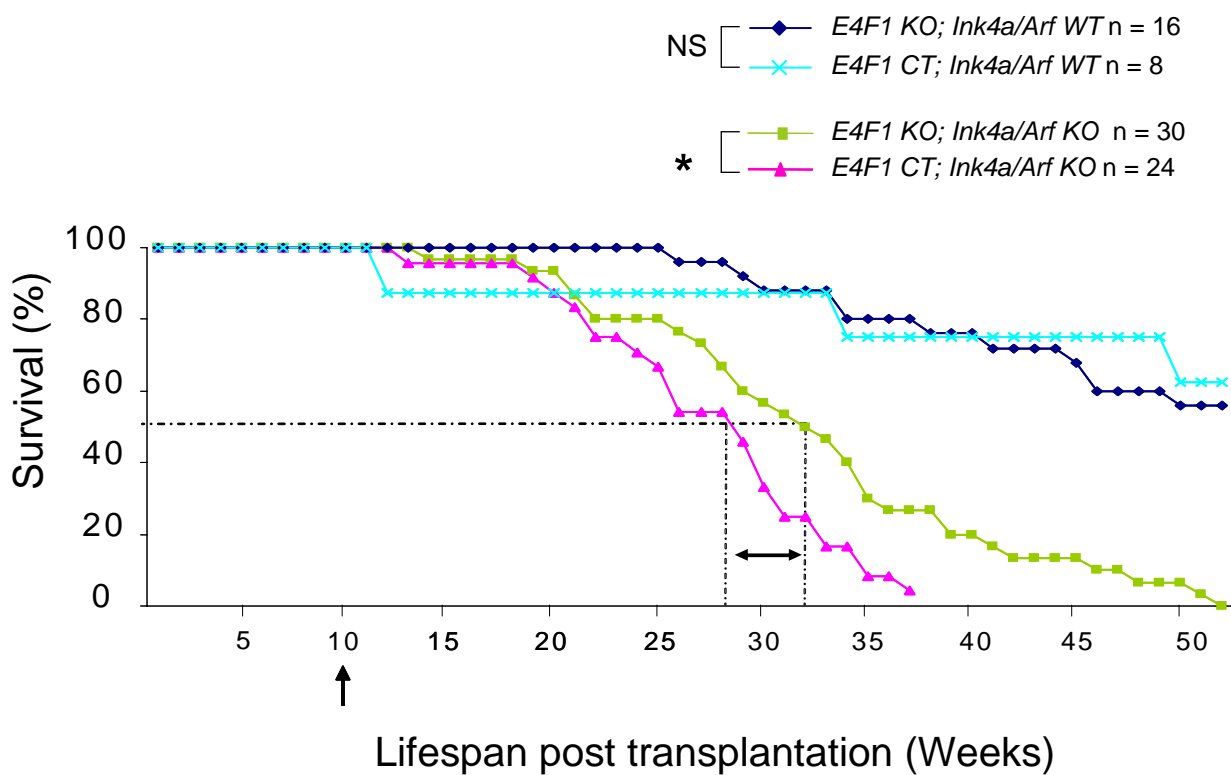
(C) Quantitative (Li-Cor technology) fluorimetric-based immunoblot analyses of E4F1 and actin protein expression levels in bone marrow samples from patients diagnosed with AML. A

representative set of 13 samples from individual patients analyzed by quantitative immunoblotting is shown. Bone marrows from healthy donors were used as controls.

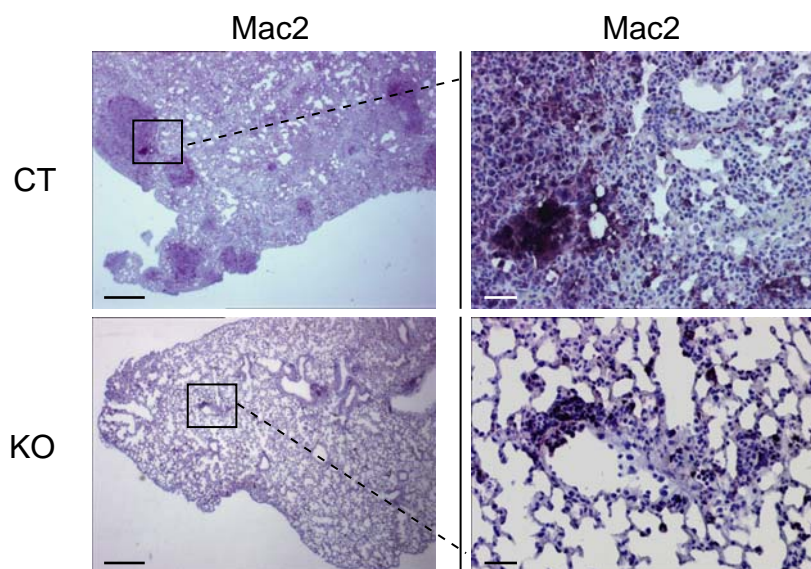
(D) shRNA-mediated depletion of E4F1 in human leukemic cell lines induces increased ROS levels. ROS levels (DFCDA) were analyzed by flow cytometry upon shRNA-mediated depletion of E4F1 in U937, HEL, HL60 and THP1 cell lines. Histograms represent quantitative analyses of 3 independent experiments (mean \pm SD), using 2 independent shRNAs.



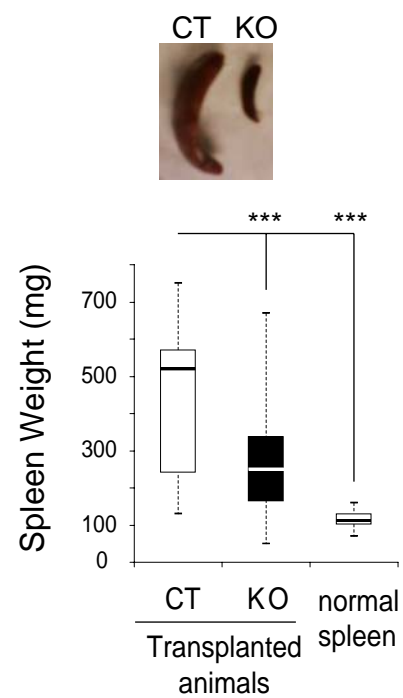
A



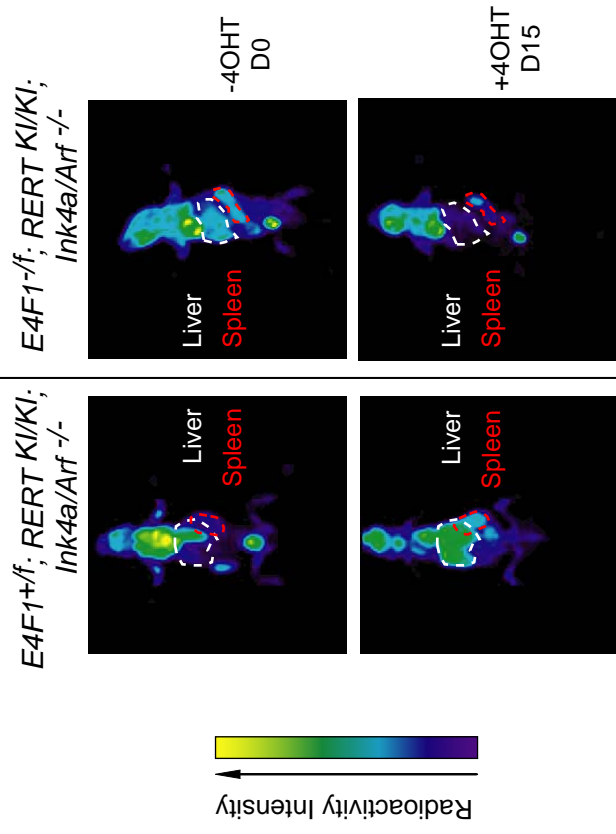
B



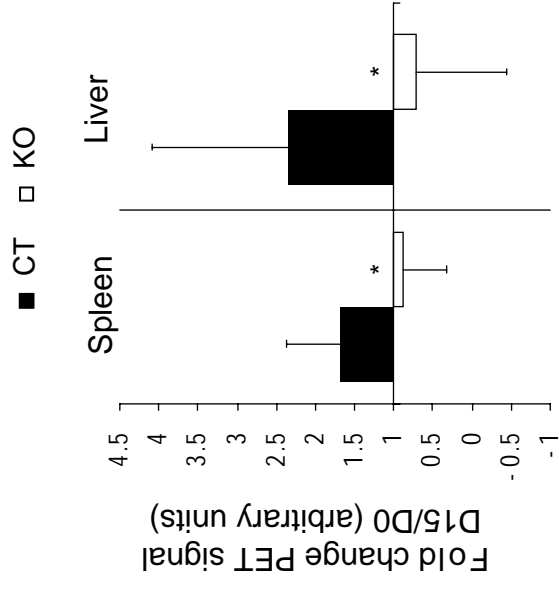
C



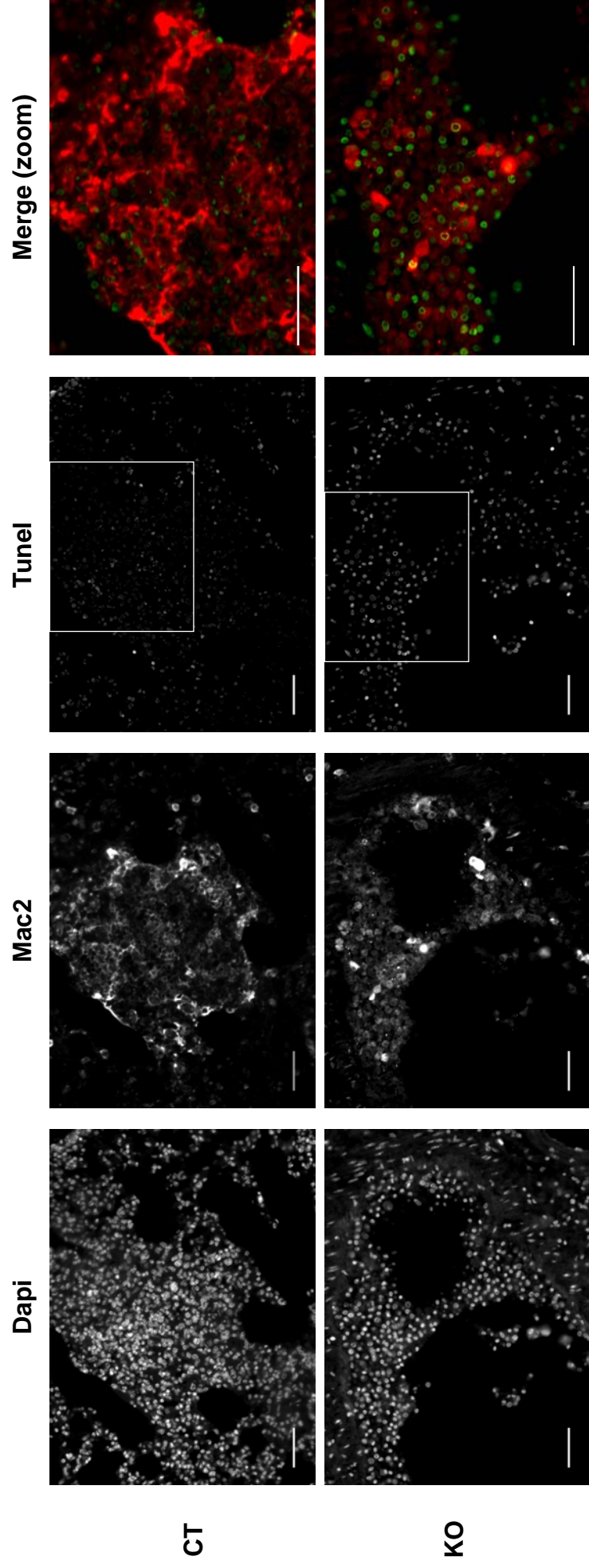
A



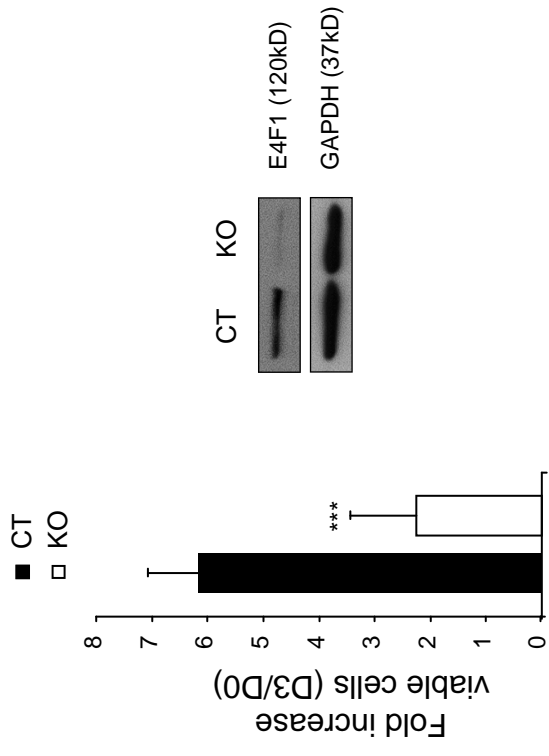
B



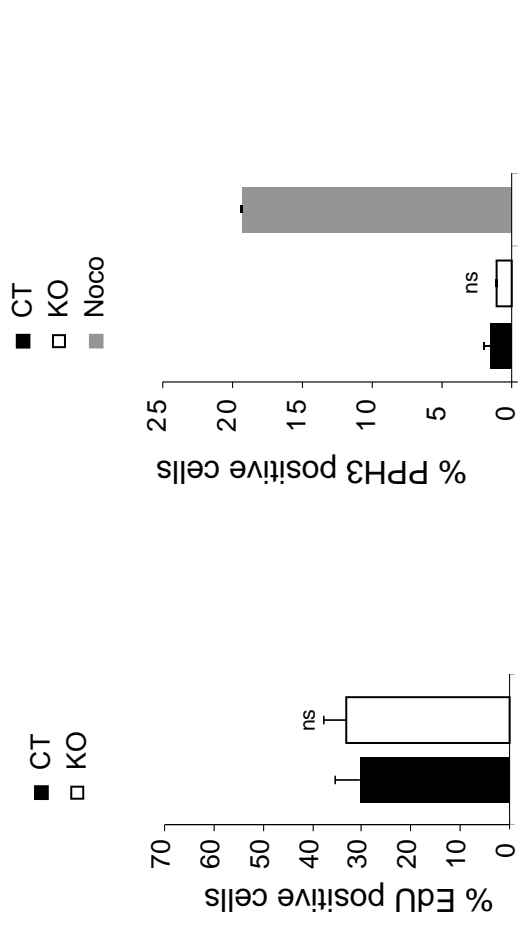
C



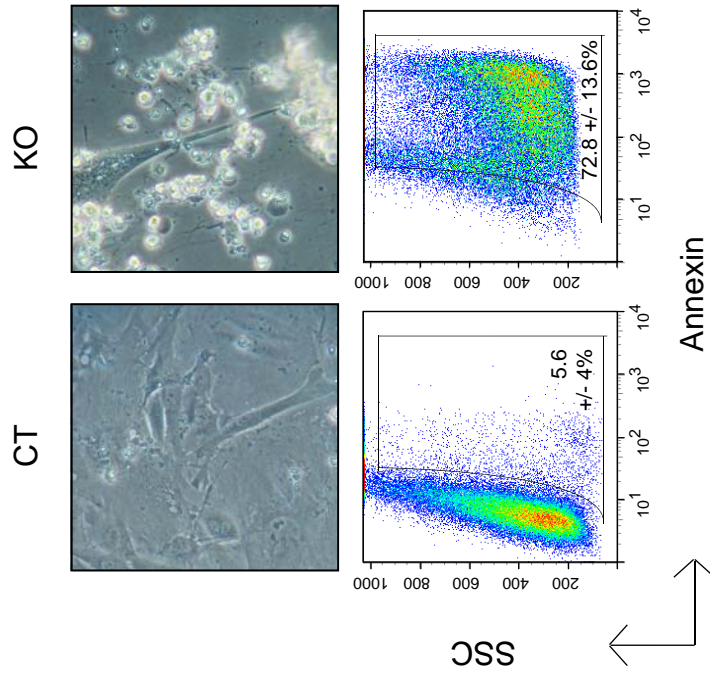
A



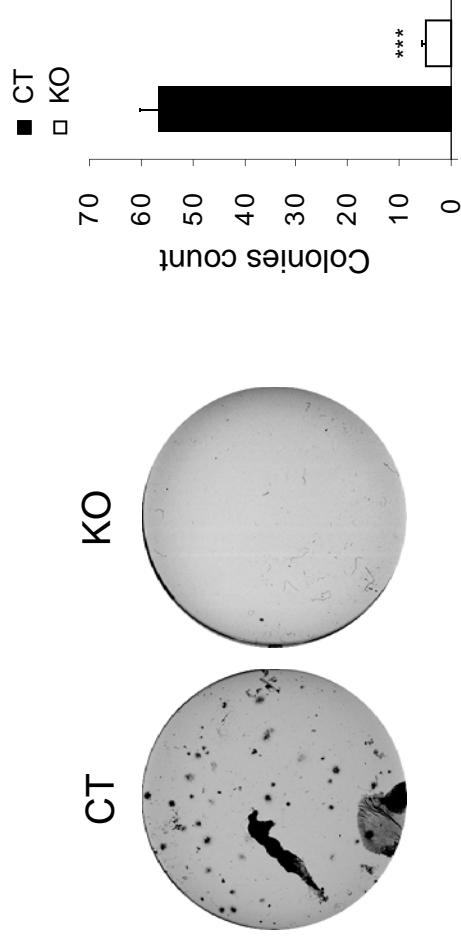
B

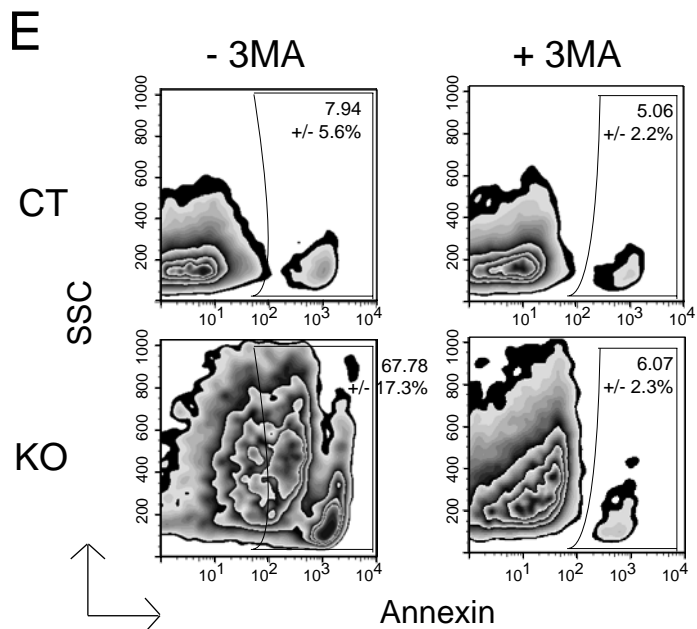
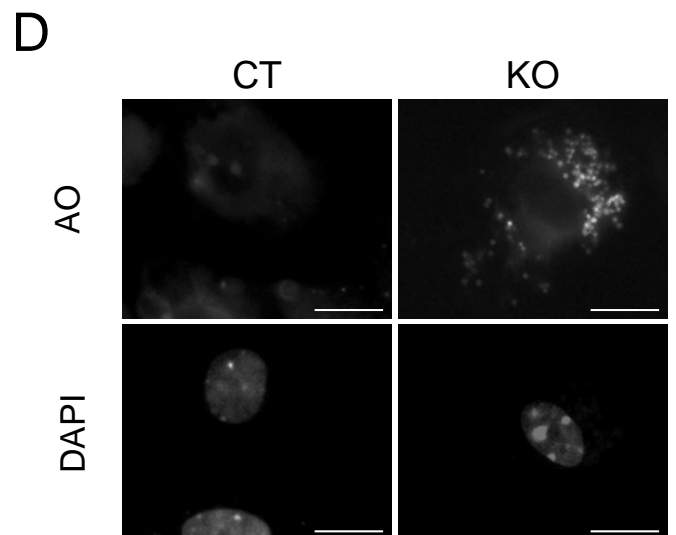
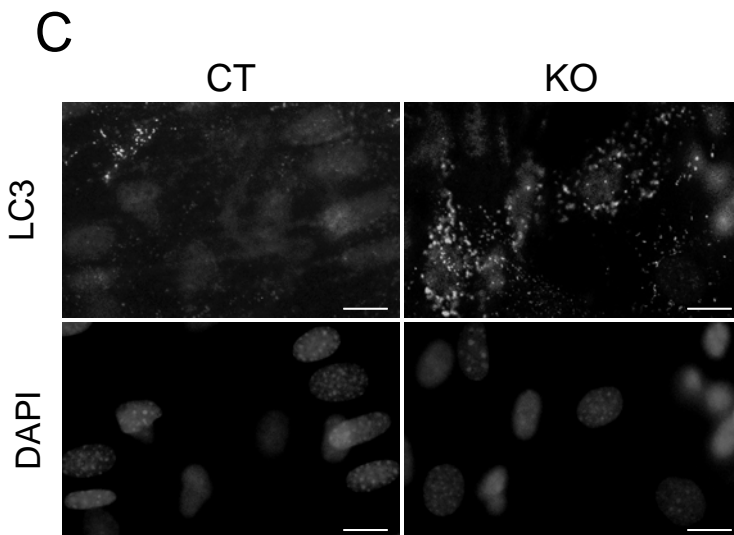
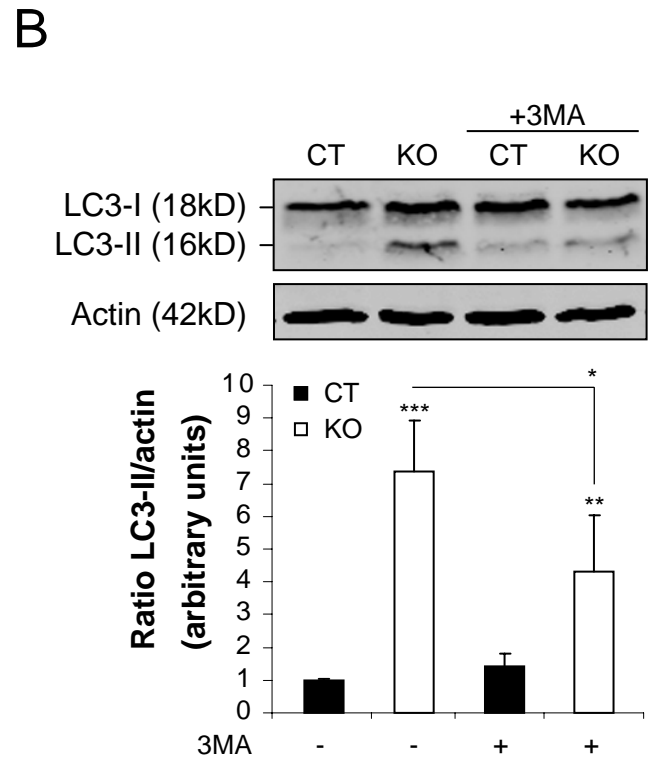
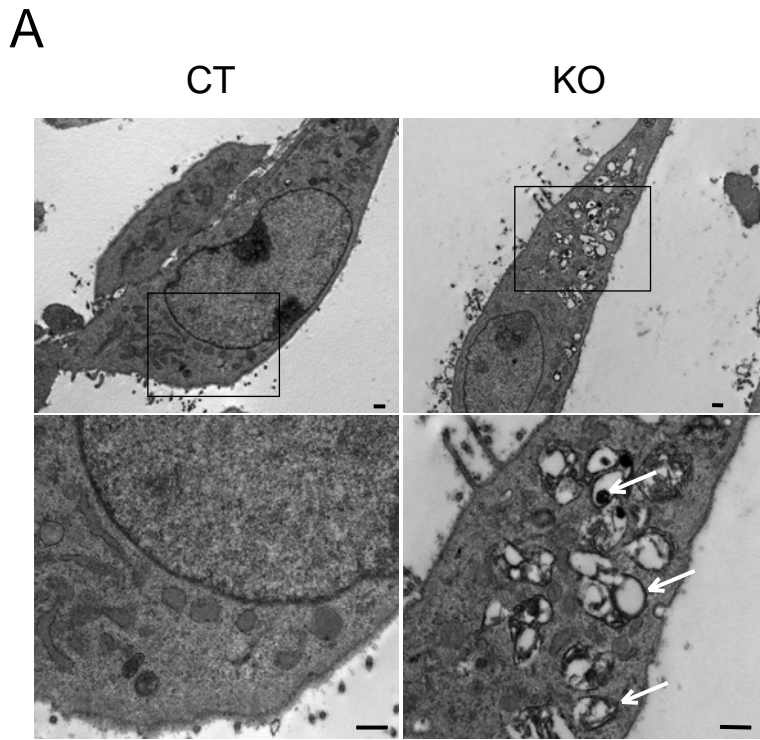


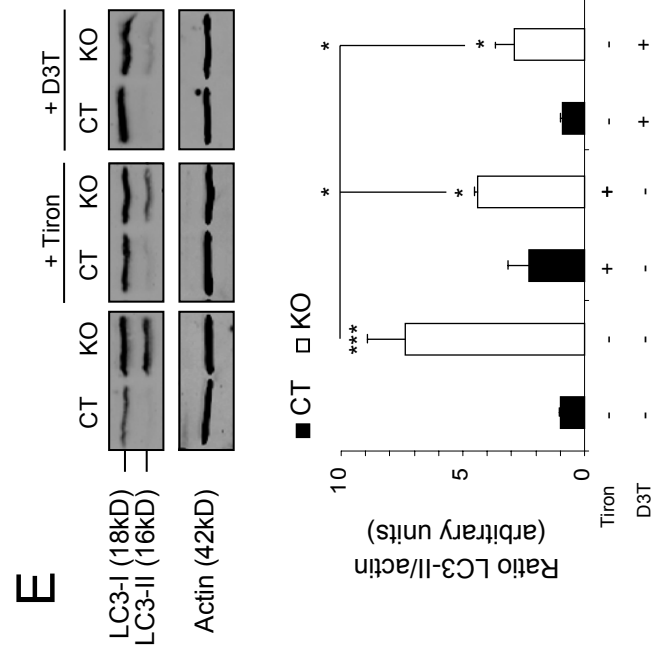
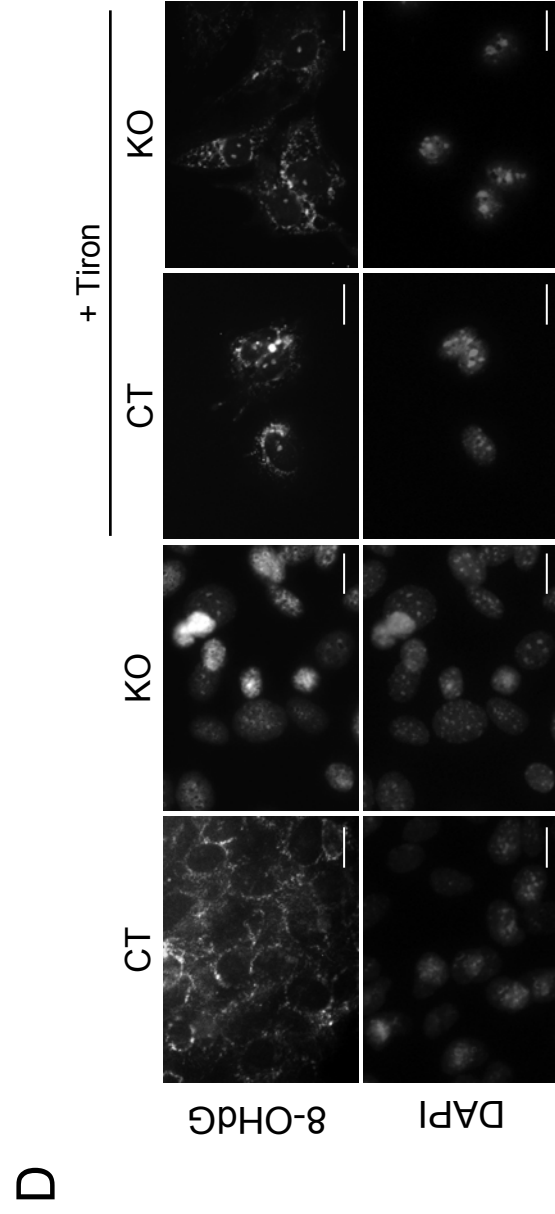
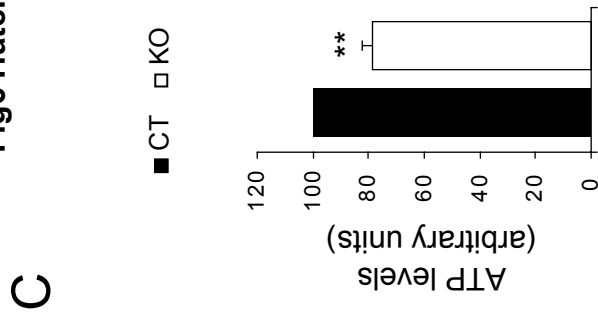
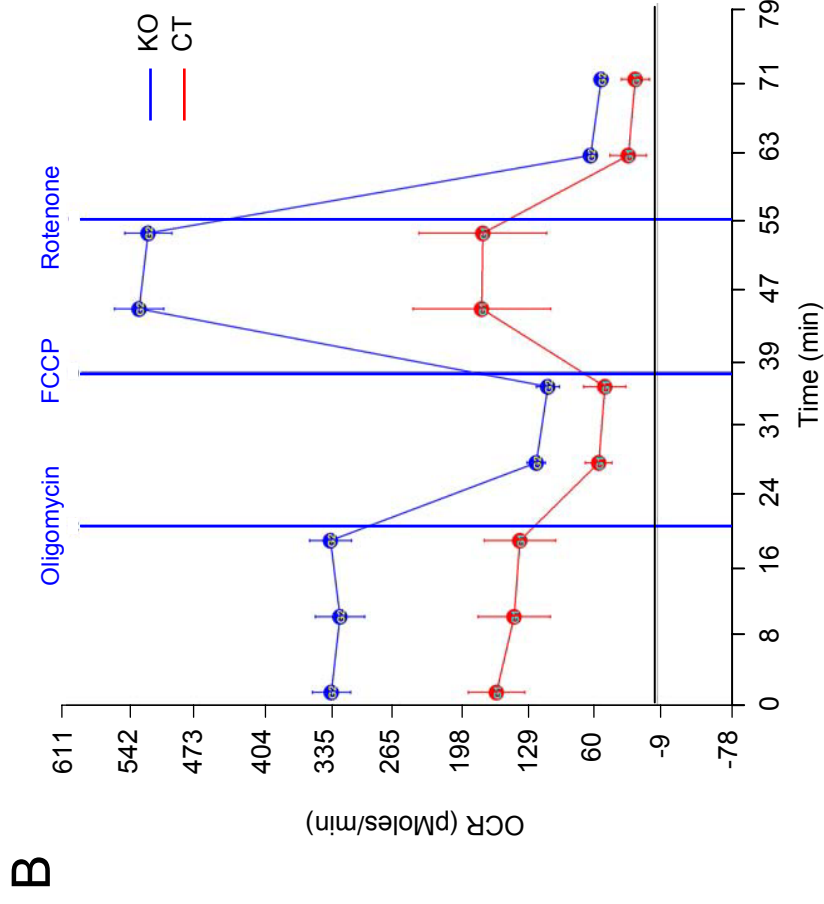
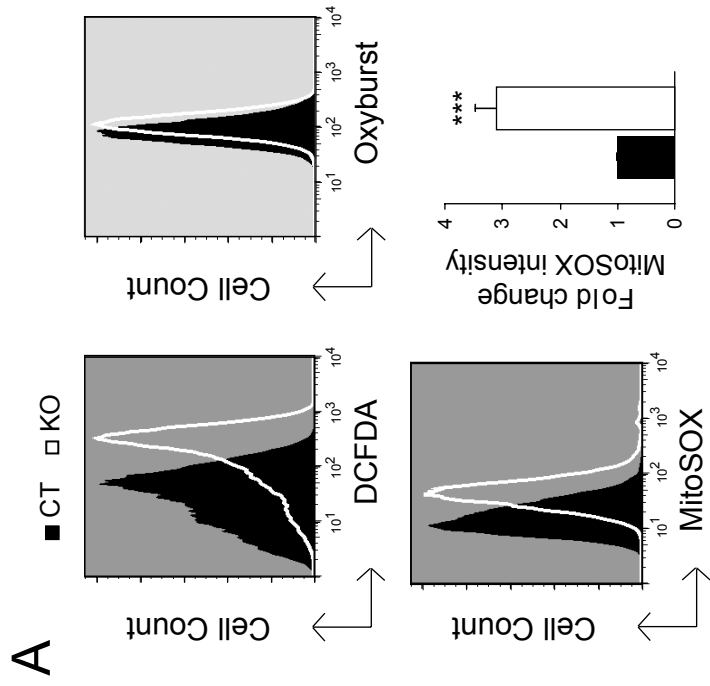
C



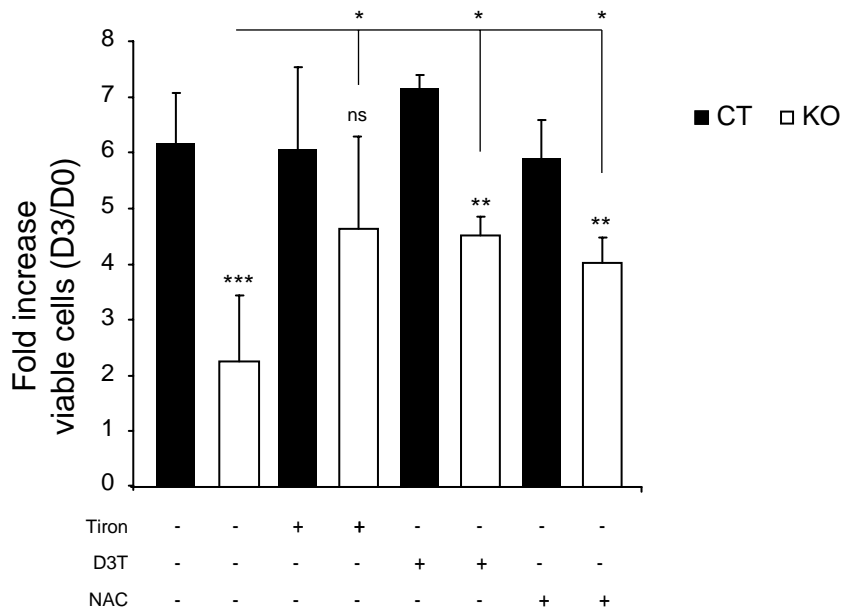
D



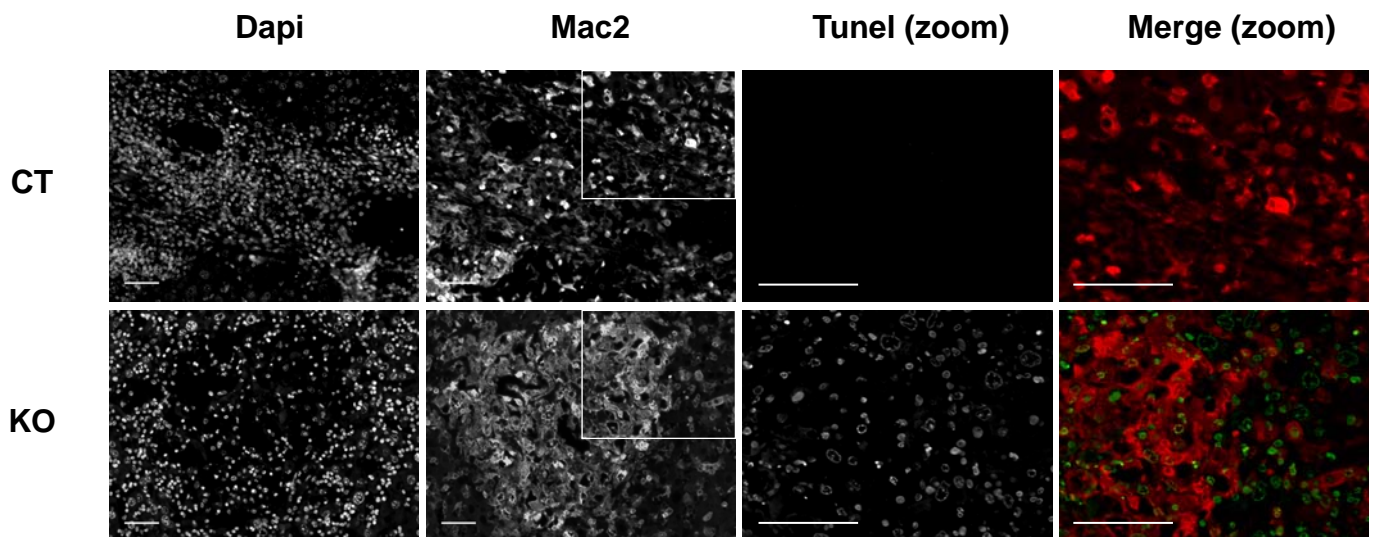




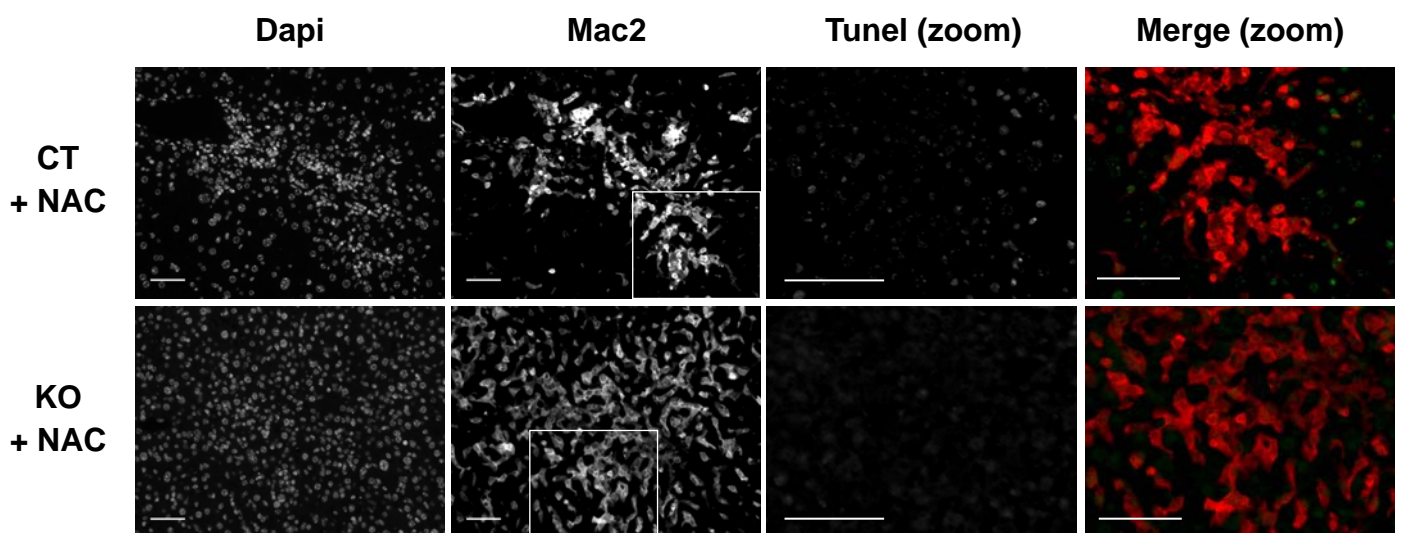
A

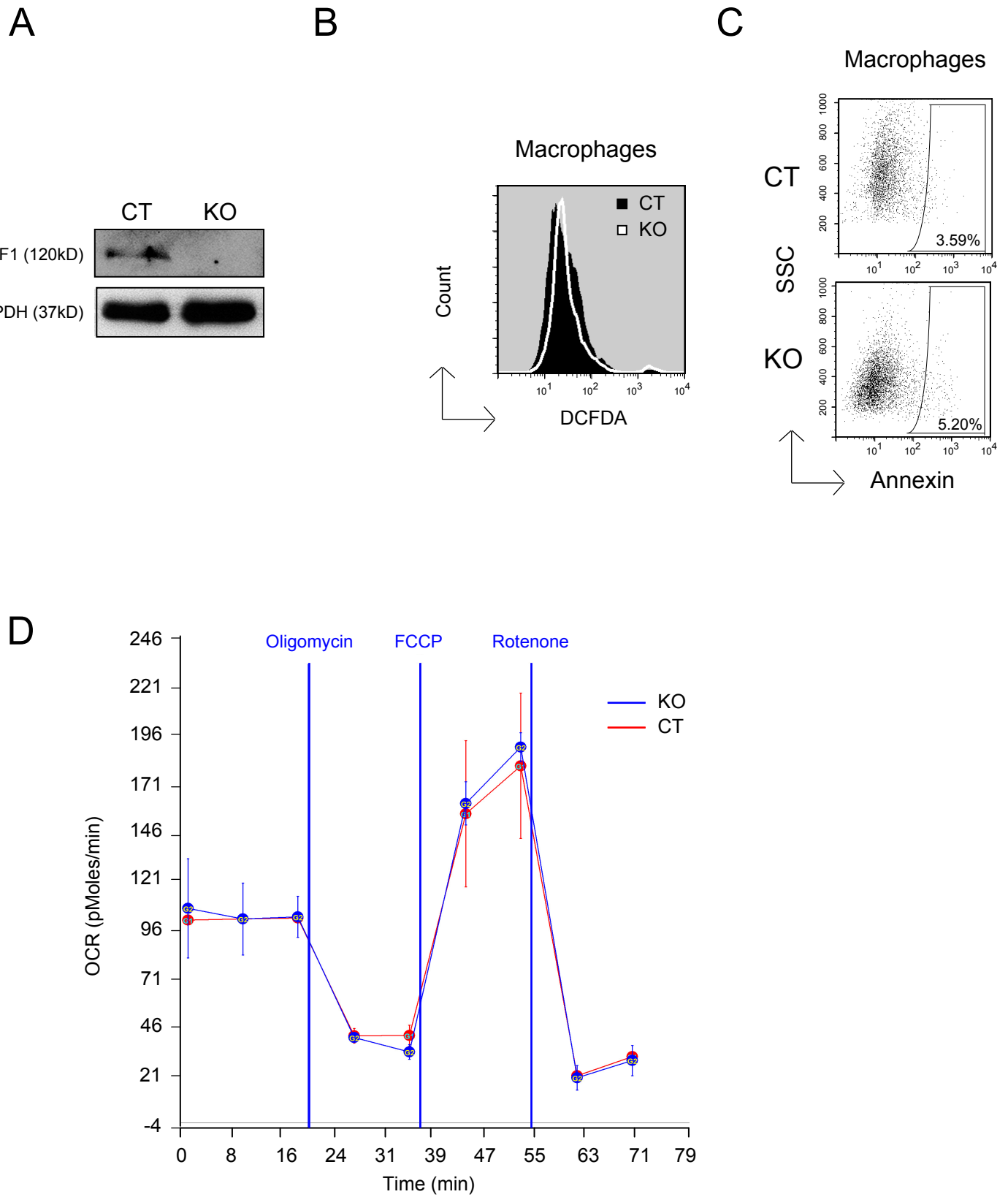


B

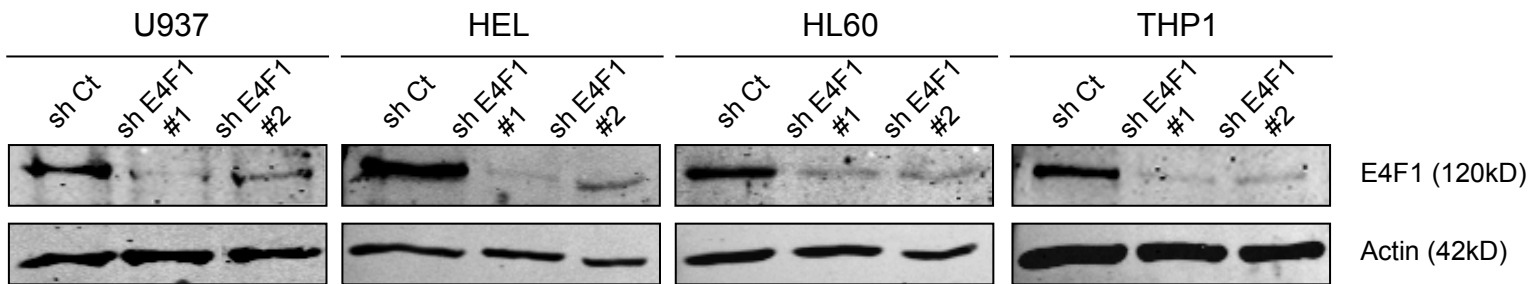


C

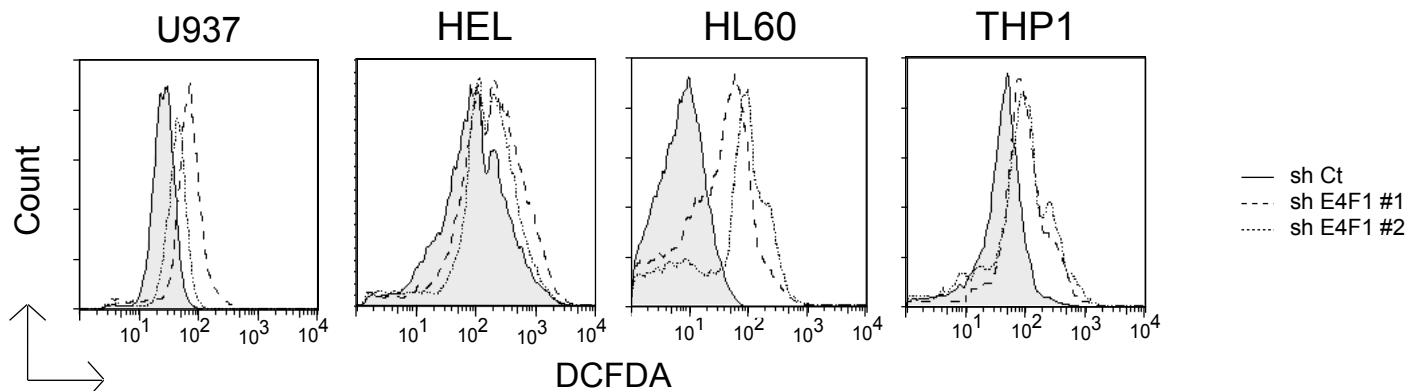




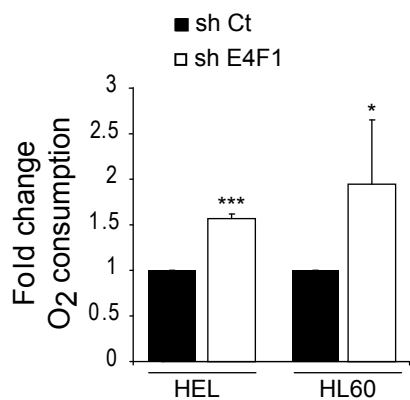
A



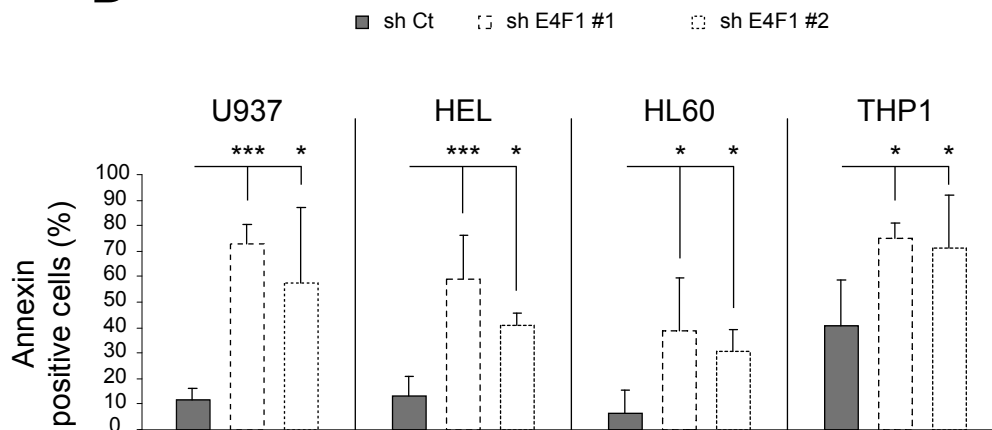
B



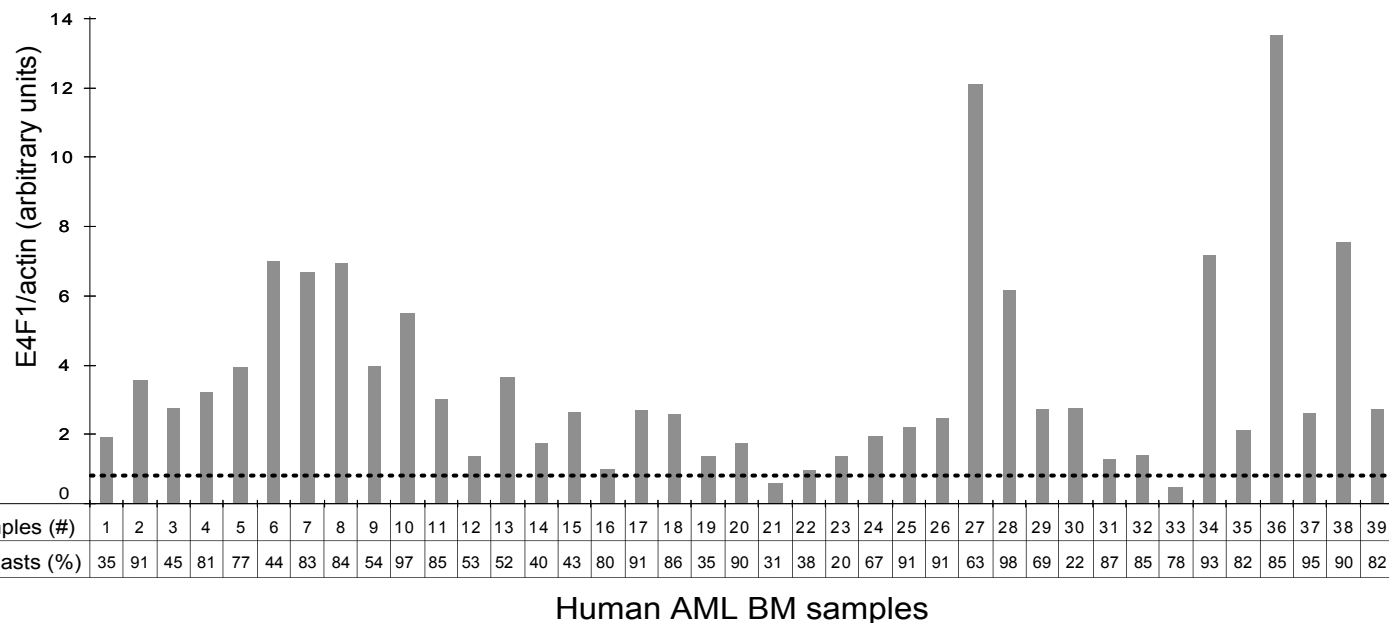
C

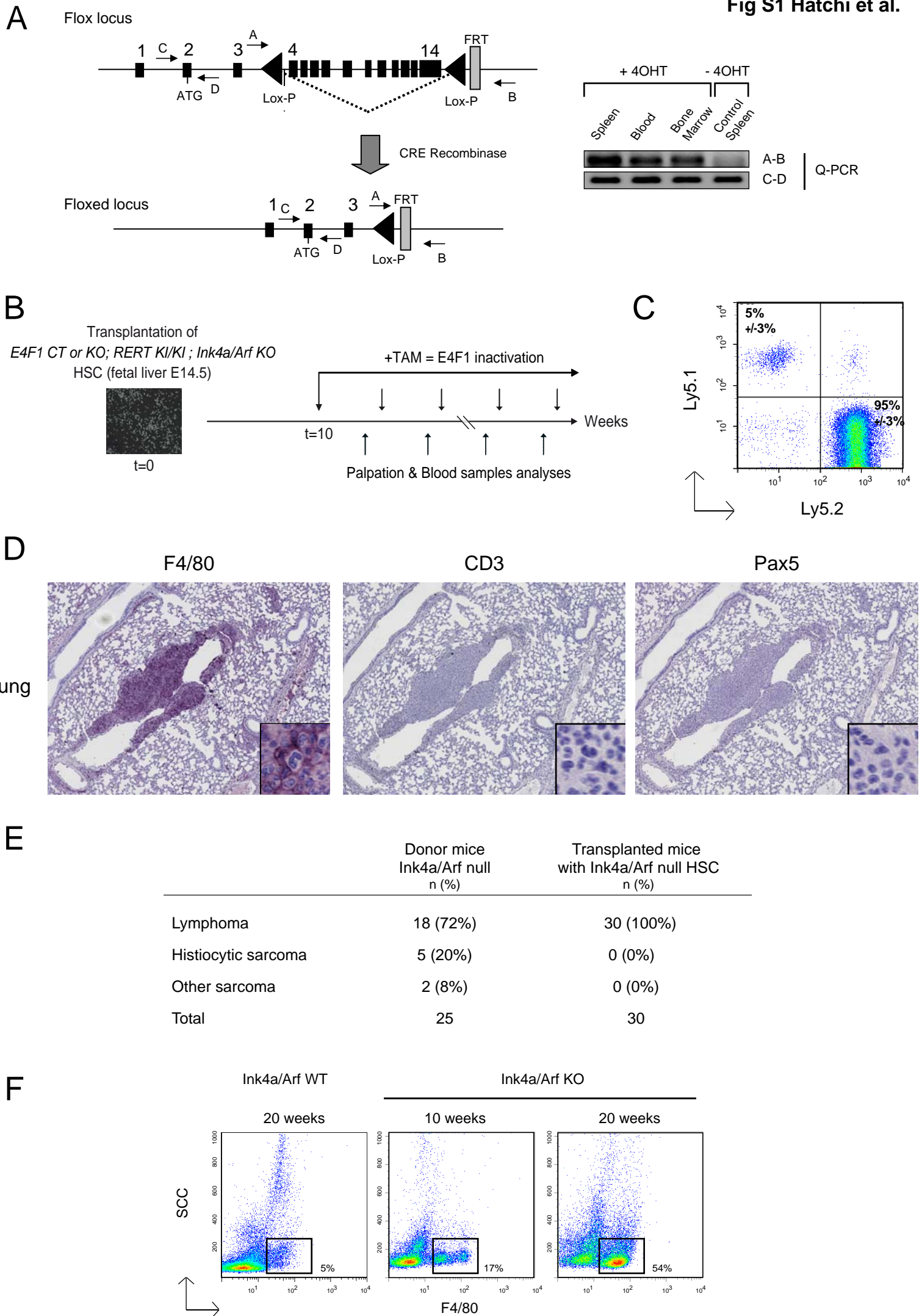


D

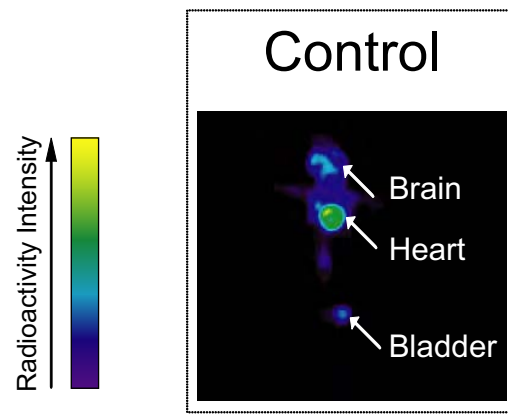


E

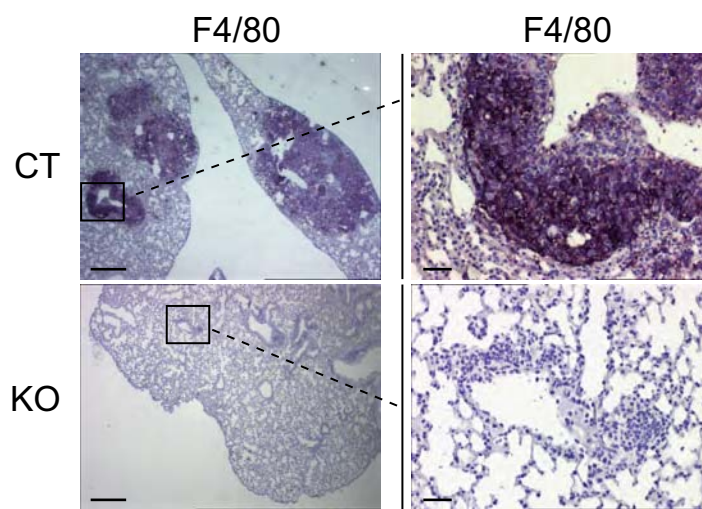




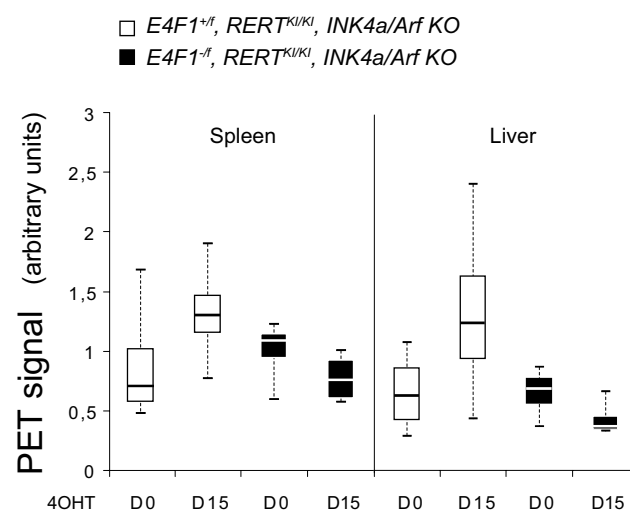
A

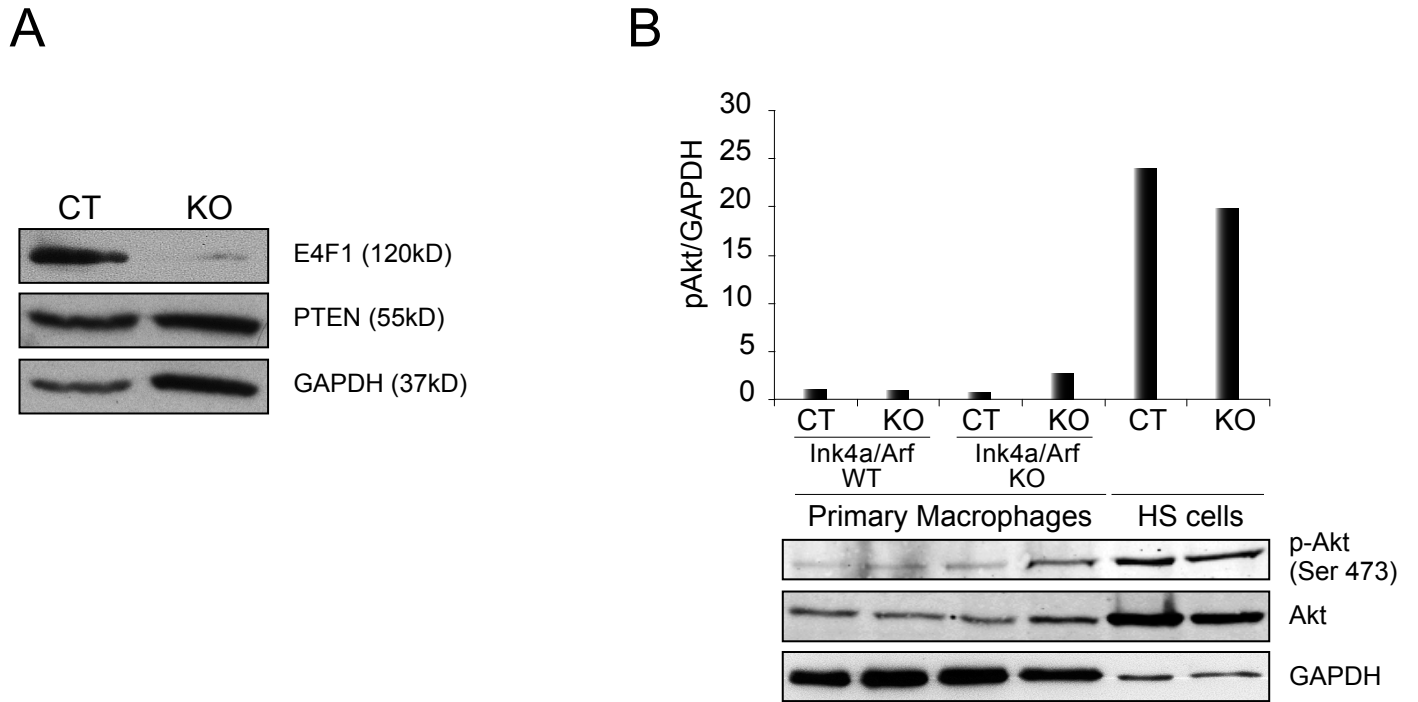


B

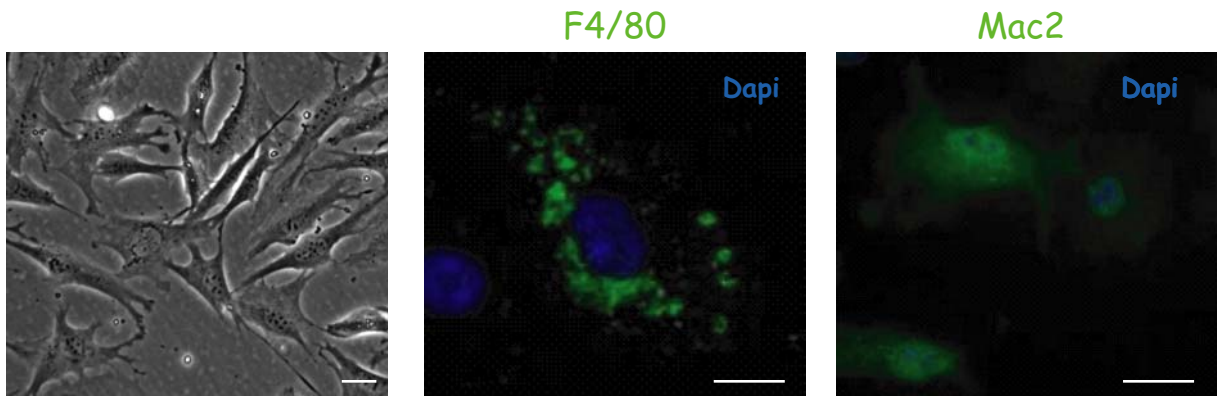


C

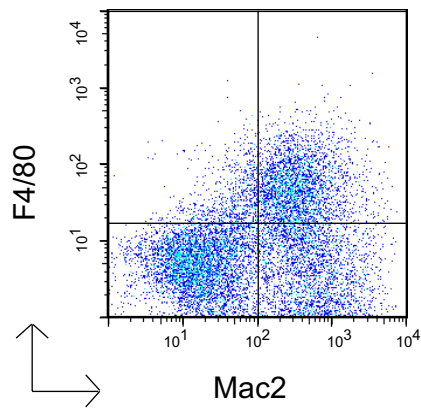




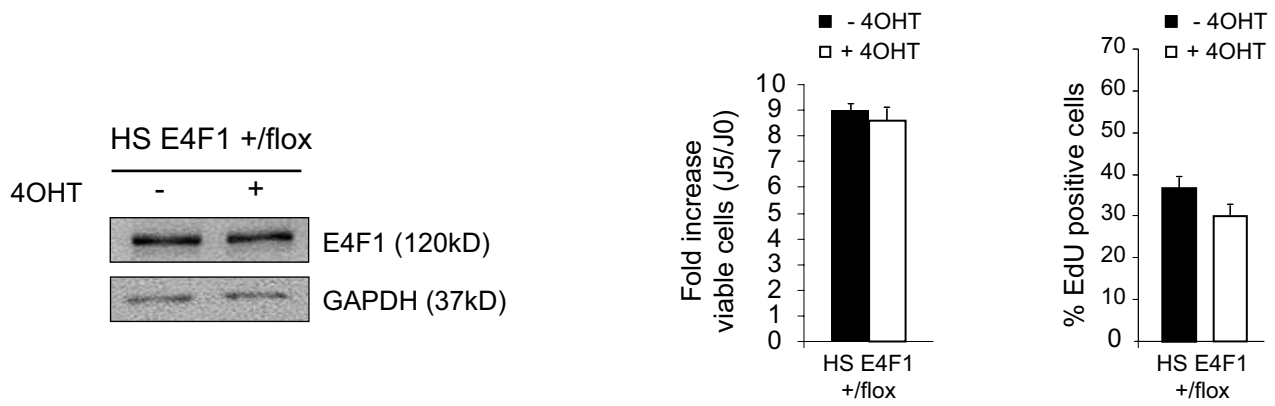
A



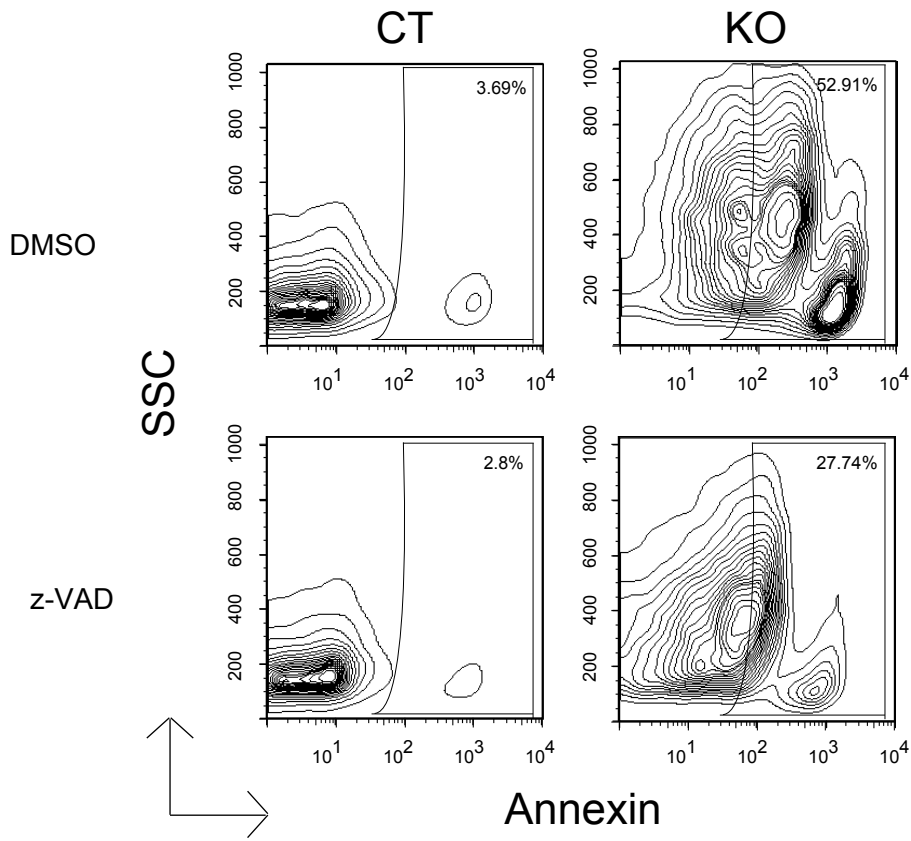
B



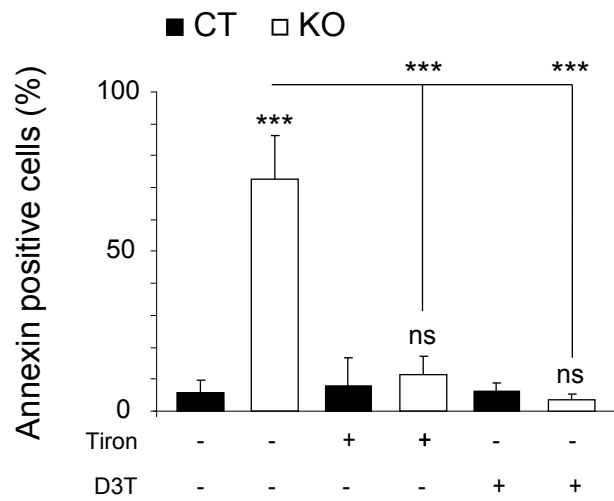
C

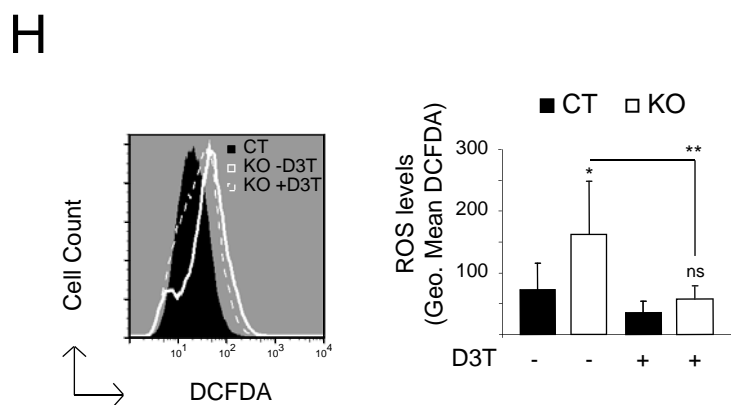
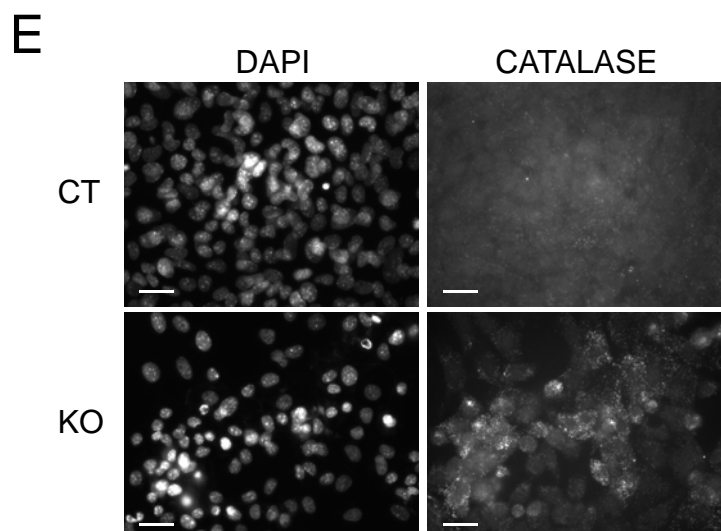
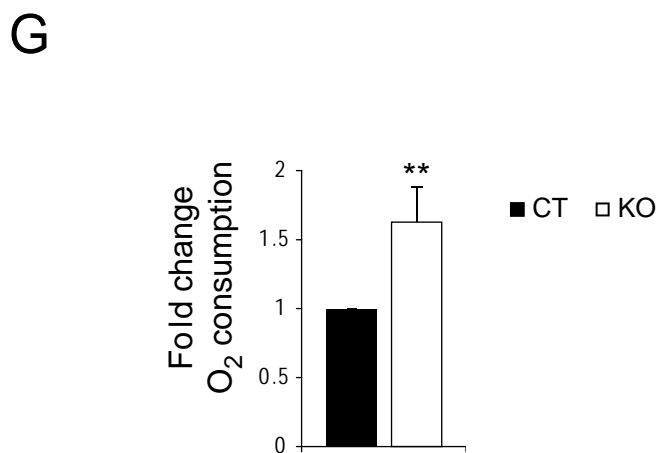
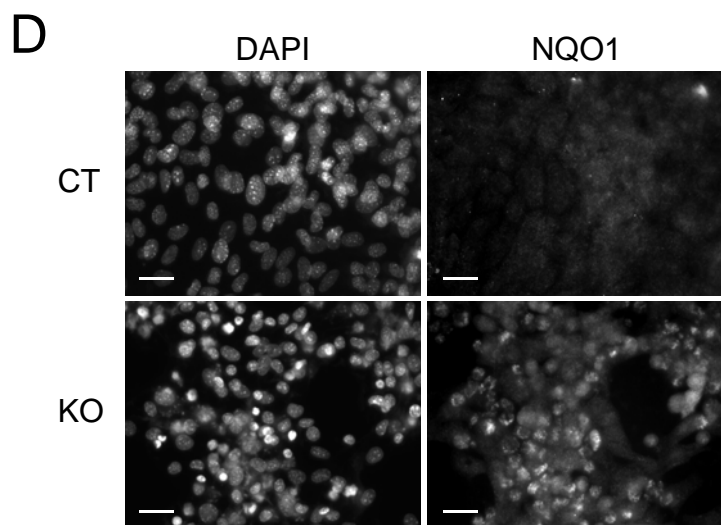
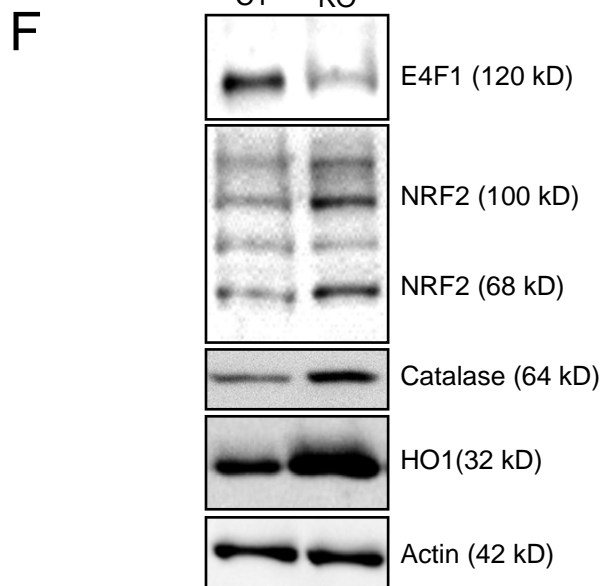
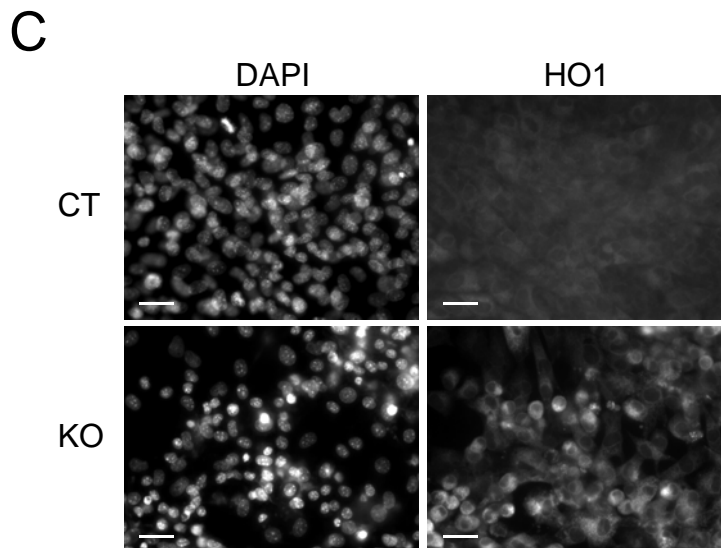
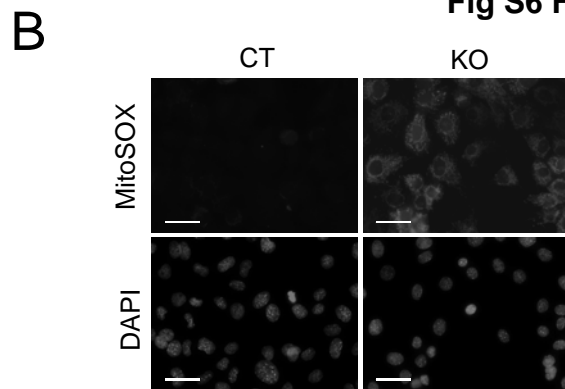
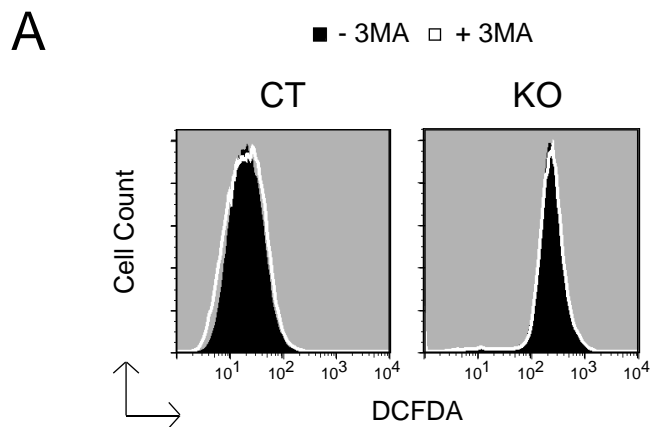


A

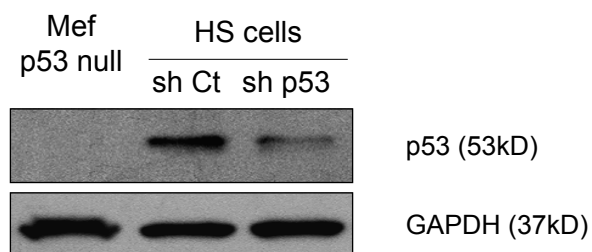


B

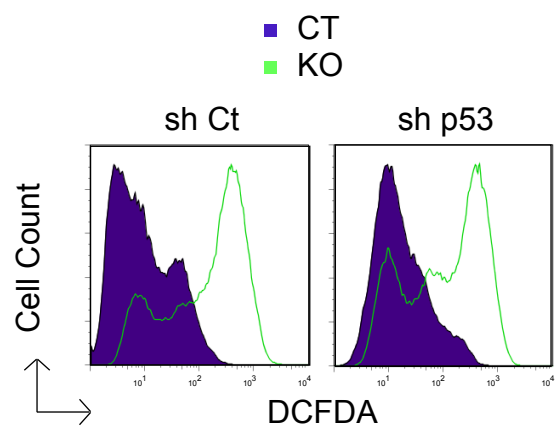




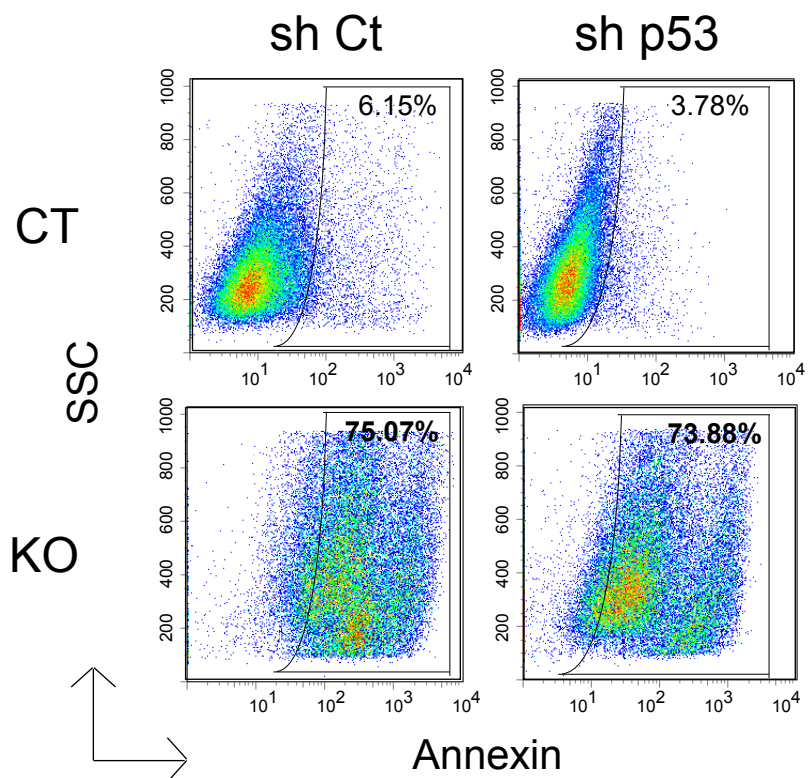
A



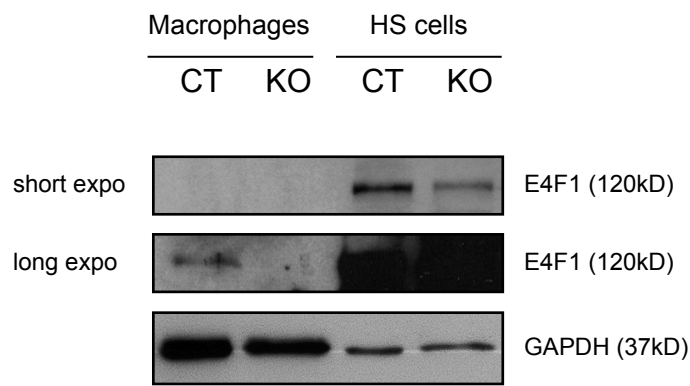
B



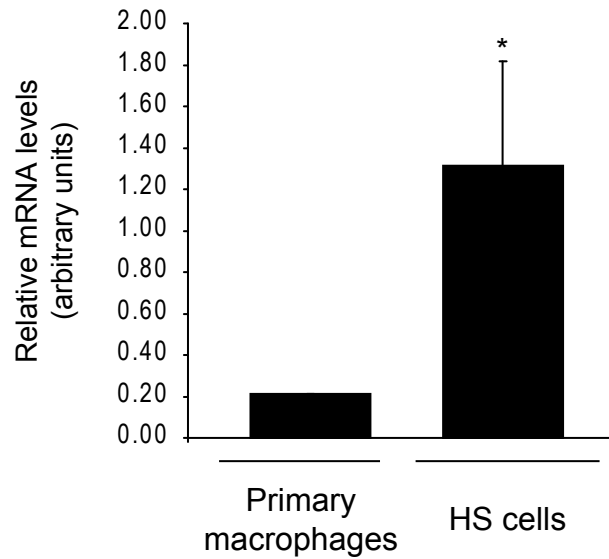
C



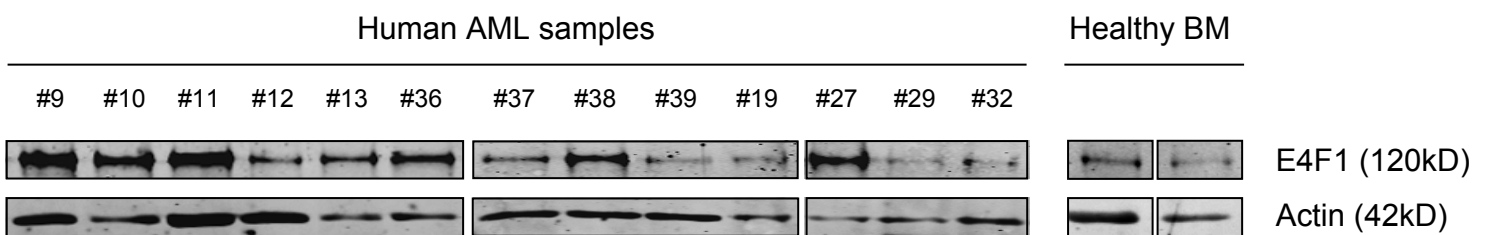
A



B



C



D

